LETTER

doi:10.1038/nature13248

Cntnap4 differentially contributes to GABAergic and dopaminergic synaptic transmission

T. Karayannis[1]*, E. Au[1]*, J. C. Patel[2], I. Kruglikov[1], S. Markx[3], R. Delorme[4,5,6], D. Héron[7], D. Salomon[8], J. Glessner[9], S. Restituito[1], A. Gordon[8], L. Rodriguez-Murillo[3], N. C. Roy[1,10], J. A. Gogos[11], B. Rudy[1], M. E. Rice[2], M. Karayiorgou[3], H. Hakonarson[4], B. Keren[12], G. Huguet[4,5,13], T. Bourgeron[4,5,13,14], C. Hoeffer[1], R. W. Tsien[1], E. Peles[8] & G. Fishell[1]

Although considerable evidence suggests that the chemical synapse is a lynchpin underlying affective disorders, how molecular insults differentially affect specific synaptic connections remains poorly understood. For instance, Neurexin 1a and 2 (*NRXN1* and *NRXN2*) and *CNTNAP2* (also known as *CASPR2*), all members of the neurexin superfamily of transmembrane molecules, have been implicated in neuropsychiatric disorders. However, their loss leads to deficits that have been best characterized with regard to their effect on excitatory cells[1,2]. Notably, other disease-associated genes such as *BDNF* and *ERBB4* implicate specific interneuron synapses in psychiatric disorders[3,4]. Consistent with this, cortical interneuron dysfunction has been linked to epilepsy, schizophrenia and autism[5,6]. Using a microarray screen that focused upon synapse-associated molecules, we identified *Cntnap4* (contactin associated protein-like 4, also known as *Caspr4*) as highly enriched in developing murine interneurons. In this study we show that Cntnap4 is localized presynaptically and its loss leads to a reduction in the output of cortical parvalbumin (PV)-positive GABAergic (γ-aminobutyric acid producing) basket cells. Paradoxically, the loss of *Cntnap4* augments midbrain dopaminergic release in the nucleus accumbens. In *Cntnap4* mutant mice, synaptic defects in these disease-relevant neuronal populations are mirrored by sensory-motor gating and grooming endophenotypes; these symptoms could be pharmacologically reversed, providing promise for therapeutic intervention in psychiatric disorders.

Having detected *Cntnap4* in developing cortical interneurons, we examined its expression at later stages of development. *In situ* hybridization revealed that it is widely but sparsely distributed in a location pattern similar to cortical interneurons. Double *in situ* hybridization demonstrated that almost all *Cntnap4*-positive cells within the somatosensory cortex are GAD67 (also known as GAD1)-positive (Fig. 1a and Extended Data Fig. 1b). Using a *Cntnap4-eGFP* knock-in allele of EFGP driven from the *Cntnap4* locus (Extended Data Fig. 1a), we assessed its expression in cortical interneuron subtypes. Analysis at postnatal day 21 (P21) revealed that many eGFP$^+$ neurons also expressed PV (47 ± 4%). Conversely, 64 ± 3% of all PV$^+$ interneurons were eGFP$^+$ (Fig. 1b and Extended Data Fig. 1d, e). The remaining 53% of *Cntnap4*-eGFP$^+$ neurons were immunopositive for other interneuron markers, reelin (RELN), VIP, NPY and calretinin, but not somatostatin (Extended Data Fig. 1c). As the mice matured, there was a steady rise in the percentage of *Cntnap4*-eGFP$^+$ PV cells. By P60 almost all PV cells expressed Cntnap4 (94 ± 3%; PV$^+$ cells as a proportion of total *Cntnap4*-eGFP$^+$ cells was 76 ± 2%) (Fig. 1b), suggesting a possible involvement of *Cntnap4* in their maturation. In addition, *Cntnap4* expression was also enriched in the substantia nigra pars compacta (SnC) and ventral tegmental area (VTA) midbrain dopaminergic projection populations. Approximately 90% of the tyrosine hydroxylase (TH)-positive dopaminergic neurons also expressed Cntnap4 (Fig. 1c).

Previously, Cntnap4 was shown to associate with presynaptic proteins such as NB-2 (also known as contactin 5), as well as Mint1 (also known as Apba1) and CASK, which are important for inhibitory synapses[7–10]. We examined pre- and postsynaptic fractions prepared from wild type and knockout *Cntnap4* animals. Cntnap4 was found to be enriched in synapses, exclusively within the presynaptic compartment (Fig. 1d). Additional verification of these results was obtained by using a fusion of extracellular Cntnap4 and Fc domains on hippocampal neuronal cultures, demonstrating the majority of Cntnap4 protein is found on the cell body and proximal dendrites in a punctate pattern, co-localized with gephyrin (Fig. 1e and Extended Data Fig. 1f). Hence, Cntnap4 is highly expressed in cortical PV cells and midbrain dopaminergic neurons and is localized presynaptically.

To assess Cntnap4 function, we generated two lines of *Cntnap4* null mice of mixed inbred background (line no. 149 and line no. 13) by replacing the first coding exon of *Cntnap4* with eGFP and a neomycin cassette (Extended Data Fig. 1a). Focusing primarily on the 149 line, we examined the functional consequences of *Cntnap4* loss on the dopaminergic and GABAergic populations. We used fast-scan cyclic voltammetry to monitor axonal dopamine spillover in the caudate putamen (CPu) and nucleus accumbens (NAc) of heterozygous, knockout and wild-type mice[11]. Dopamine release was evoked by single or brief pulse trains (20 pulses at 10 Hz or 5 pulses at varying frequencies). Both heterozygous and knockout mice compared to wild-type animals, showed an increase in peak extracellular dopamine concentration ($[DA]_o$) that was more pronounced in the NAc than CPu, especially with multiple pulse stimulation (Fig. 2a). Moreover, evoked $[DA]_o$ was enhanced evenly across frequencies varying from 5 to 100 Hz (Extended Data Fig. 2a) indicating both tonic and phasic firing are affected. Analysis of the maximum dopamine uptake rate, V_{max}[12], revealed that the rates were somewhat higher in heterozygous and knockout animals compared to wild type (CPu: 7.48 ± 0.30 μM s^{-1} mutants versus 7.25 ± 0.43 μM s^{-1} in wild type; NAc: 5.39 ± 0.23 μM s^{-1} mutants versus 4.95 ± 0.23 μM s^{-1} in wild type). However, the excitability of dopaminergic neurons between knockout and wild-type cells appeared unaffected (data not shown). Hence, increased evoked $[DA]_o$ in *Cntnap4* mutants does not appear to be a consequence of impaired dopamine transporter activity or intrinsic

[1]Department of Neuroscience and Physiology, NYU Neuroscience Institute, New York, New York 10016, USA. [2]Department of Neurosurgery, Neuroscience and Physiology, New York University Langone Medical Center, New York, New York 10016, USA. [3]Department of Psychiatry, College of Physicians and Surgeons, Columbia University, 1051 Riverside Drive, New York, New York 10032, USA. [4]Institut Pasteur, Human Genetics and Cognitive Functions Unit, 75724 Paris, France. [5]CNRS URA 2182 Genes, Synapses and Cognition, Institut Pasteur, 75724 Paris, France. [6]Assistance Publique-Hôpitaux de Paris, Robert Debré Hospital, Department of Child and Adolescent Psychiatry, 75019 Paris, France. [7]Unité Fonctionnelle de Génétique Médicale AP-HP, Département de Génétique et Cytogénétique, Centre de Référence, Déficiences intellectuelles de causes rares, CRicm, UMR-S975, Groupe Hospitalier Pitié-Salpêtrière, F-75013, Paris, France. [8]Department of Molecular Cell Biology, Weizmann Institute of Science, Rehovot 76100, Israel. [9]Center for Applied Genomics, The Children's Hospital of Philadelphia, Philadelphia, Pennsylvania 19104, USA. [10]Section on Synaptic Transmission, National Institute on Deafness and Other Communication Disorders, National Institutes of Health, Bethesda, Maryland 20892, USA. [11]Departments of Physiology and Cellular Biophysics and Neuroscience, Columbia University Medical Center, New York, New York 10032, USA. [12]Unité Fonctionnelle de Génétique Chromosomique AP-HP, Département de Génétique et Cytogénétique, CRicm, UMR-S975, Groupe Hospitalier, Pitié-Salpêtrière, 75013 Paris, France. [13]University Paris Diderot, Sorbonne Paris Cité, Human Genetics and Cognitive Functions, 75005 Paris, France. [14]FondaMental Foundation, 94000 Créteil, France.
*These authors contributed equally to this work.

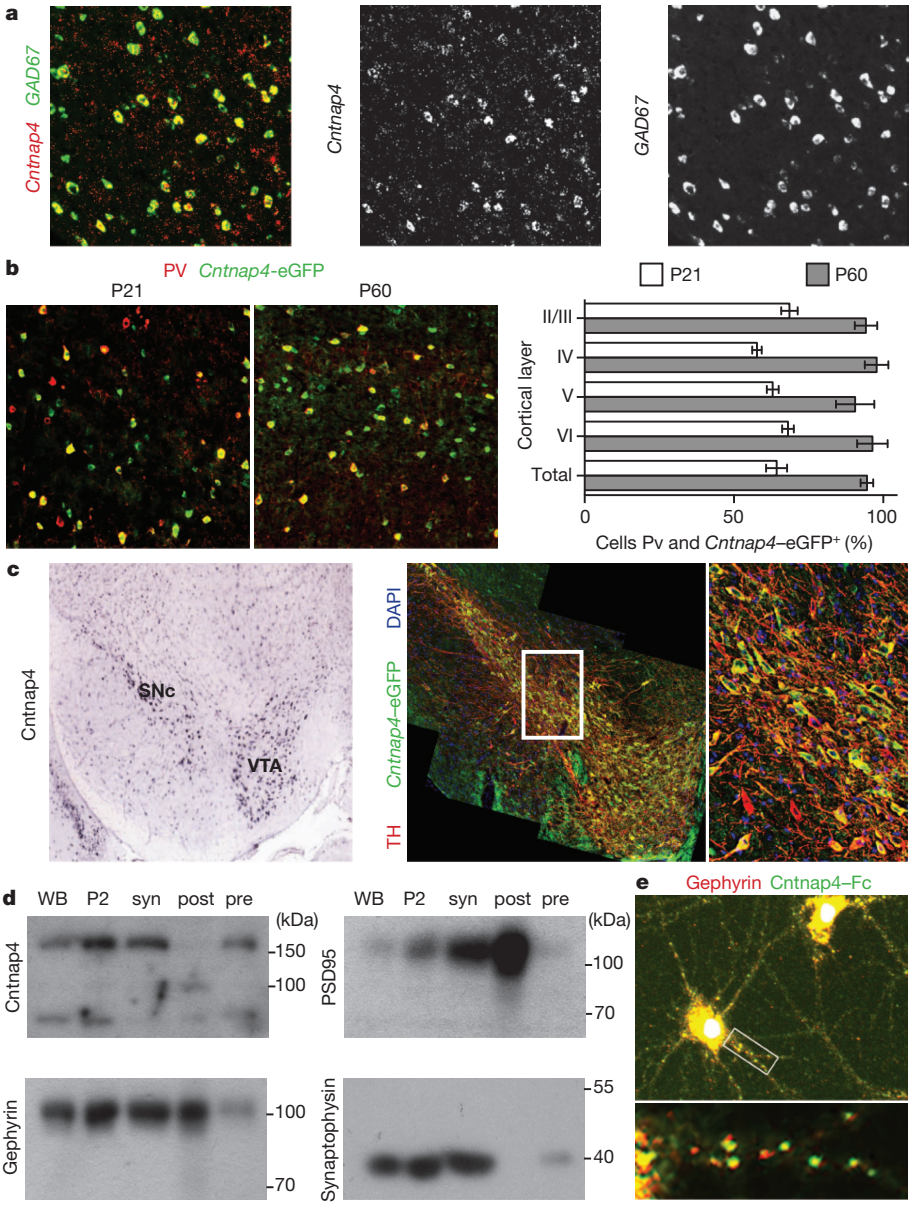

Figure 1 | Cellular and subcellular localization of Cntnap4. **a**, Double fluorescent *in situ* hybridization on P21 wild-type somatosensory cortex with co-localization of *Cntnap4* (green) and *GAD67* (red). **b**, Overlap between parvalbumin (PV) (red) and Cntnap4 (eGFP knock-in) at P21 and P60. **c**, *In situ* hybridization of Cntnap4 in VTA and SNc of adult WT (©2014 Allen Institute for Brain Science. Allen Mouse Brain Atlas [Internet]. Available from: http://mouse.brain-map.org/) and *Cntnap4*-eGFP (green) co-localization with tyrosine hydroxylase (red) at P21. Close-up of the area within the white box is shown on the right. **d**, Western blots on whole brain (WB), total membrane (P2), synaptosomes (syn), presynaptic (pre) and postsynaptic (post) compartments. Cntnap4 present at presynaptic site (pre). Internal controls for pre- (synaptophysin) and post-synaptic (gephyrin and PSD95) fractions (3 biological replicates, $n = 3$ brains each replicate). **e**, Cntnap4–Fc fusion protein (green) binds to soma and proximal dendrites, apposed to gephyrin puncta (red) in dissociated cortical neurons (3 biological replicates, $n = 10$ coverslip cultures analysed).

electrophysiological properties. We conclude that Cntnap4 normally acts to attenuate dopamine release through a presynaptic mechanism.

Given the dopamine findings, we expected that GABAergic signalling would also be elevated in mutant mice. However, in *Cntnap4* knockout animals compared to controls, spontaneous inhibitory postsynaptic currents (sIPSCs) in pyramidal cells were fewer, smaller and slower (Extended Data Fig. 2b). Intriguingly, paired-cell recordings between PV and excitatory cells in three-week-old knockout mice had synaptic responses reminiscent of those in immature fast spiking (FS) cells[13] (Fig. 2b). IPSC amplitude was reduced and kinetics were prolonged, with longer rise-times and decay tau values (Fig. 2b, c and Extended Data Fig. 2c). In addition, the average latency of the IPSCs was marginally increased and between-trials variability (jitter) was larger (Fig. 2b, c). Some of these defects persisted into adulthood and hence were not due to developmental delay (Extended Data Fig. 3a). By comparing *Cntnap4*-positive and *Cntnap4*-negative PV interneurons at P21 (Fig. 2c) we observed that negative cells resembled mutant neurons. This indicates not only that the defects we saw are cell-autonomous (*Cntnap4*-negative PV-positive interneurons, grey symbols versus *Cntnap4* knockout cells, red symbols, Fig. 2c), but also that Cntnap4 appears necessary for the full maturation of the output of PV-positive interneurons.

We then sought to address the mechanism by which the loss of *Cntnap4* affects the function of PV interneurons. A change in the probability of release seems unlikely as the paired pulse ratios in heterozygous and knockout PV interneurons were unchanged (Extended Data Fig. 2d). Moreover, no obvious differences in intrinsic firing properties, morphology or synaptogenesis between wild type, heterozygous and knockout animals (Extended Data Fig. 4a–c) were observed. Another possible mechanism is a failure to transition from N-type to P/Q-type presynaptic calcium channels[13,14]. However, application of the specific N-type calcium channel blocker ω-conotoxin GVIA in knockout paired recordings ($n = 3$) produced no change in postsynaptic responses (Extended Data Fig. 2e). Yet another possibility is that Cntnap4 affects the localization of postsynaptic $GABA_A$ receptors. Protein samples from P60 Cntnap4 wild-type and knockout cortex were sub-fractionated and tested by western blot for levels of $GABA_A$-γ2 (probes for synaptically localized $GABA_A$ receptors) as well as $GABA_A$-α1 (enriched in FS-pyramidal synapses) and, if anything, we observed a slightly elevated level for both receptor subunits in Cntnap4 knockout samples (Extended Data Fig. 4d). As Cntnap proteins help localize glycosyl phosphatidylinositol (GPI)-anchored cell adhesion molecules[15] and neurexins[16] have a structural adhesion role at the synapse, we examined symmetric perisomatic

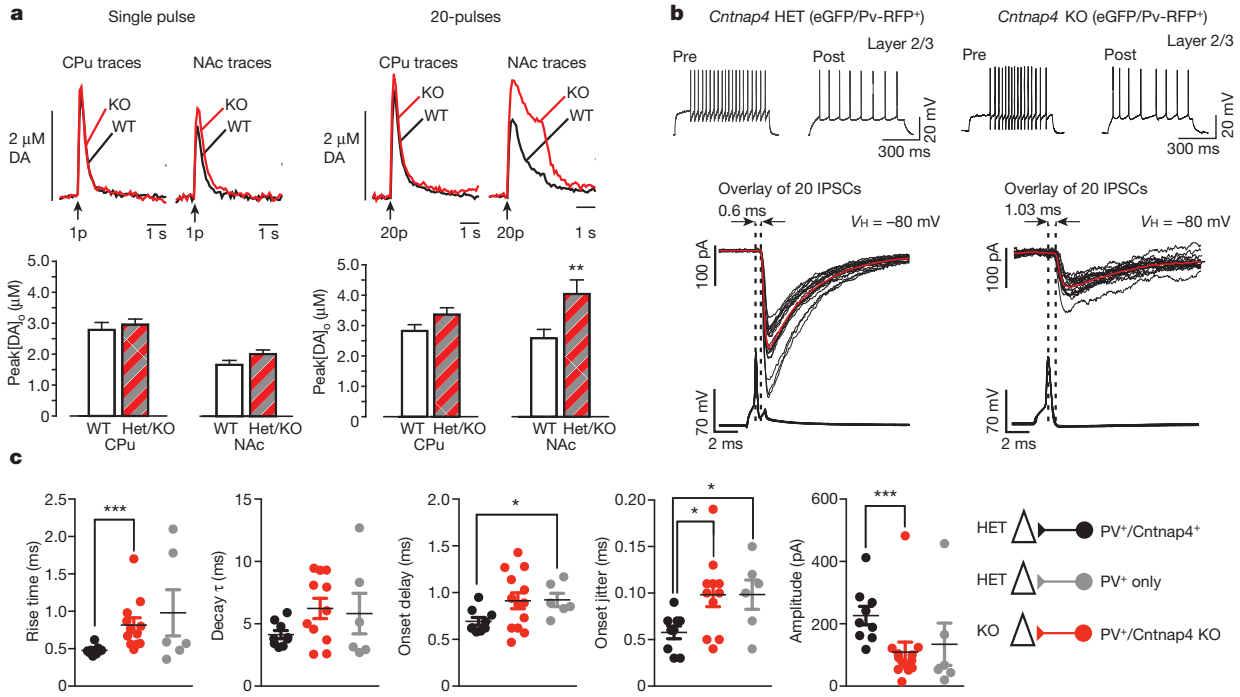

Figure 2 | *Cntnap4* mutant mice show increased dopamine but decreased GABA signalling. **a**, Evoked dopamine measurements by voltammetry *in vitro* in wild type and *Cntnap4* mutants. Increased extracellular dopamine release in mutants versus wild type. Twenty pulses lead to a significant increase in NAc. Representative traces of extracellular dopamine concentration levels $[DA]_o$ over time of wild type (black) versus knockout mice (red). Distribution of peak $[DA]_o$ values for all the data points included in the analysis ($n = 3$ for each genotype). **b**, Paired recordings between PV-positive and excitatory cells in somatosensory cortex *in vitro*. Examples of firing in pre- and postsynaptic cells upon step depolarization. A single action potential evokes fast, reliable postsynaptic responses in heterozygotes. Responses were smaller, slower and more unreliable in knockouts (individual traces are shown in grey and the average shown in red). **c**, Overall data of synaptic values for responses recorded in three groups of paired recordings. Black denotes presynaptic Cntnap4-positive PV cells in heterozygous mice; grey denotes PV cells yet to express Cntnap4 in heterozygous mice and red denotes PV cells in knockout mice ($n = 7$ brains for each HET and KO; $n = 9$ for black, $n = 13$ for red, $n = 6$ for grey paired recordings; Mann–Whitney *U*-test).

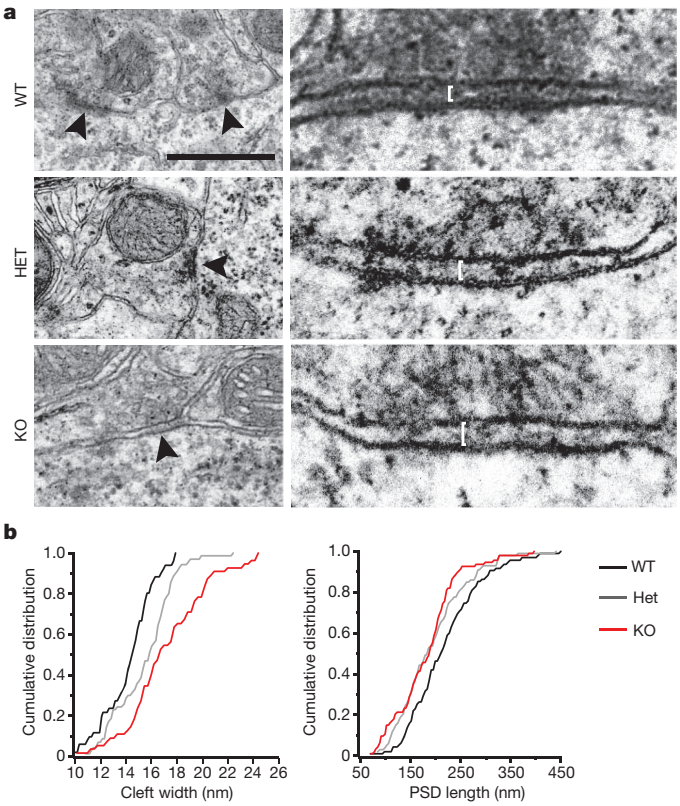

Figure 3 | Loss of Cntnap4 results in ultrastructural deficits in perisomatic inhibitory synapses. **a**, Electron micrographs of symmetric perisomatic synaptic contacts (black arrowheads) in wild type (WT), heterozygous (Het) and knockout (KO) littermate mice. Higher magnification shown on right (white bars indicate cleft width). Scale bar, 500 nm. **b**, Cumulative distributions of cleft width and PSD length. (PSD width of WT versus KO $P < 0.0001$; WT versus HET $P = 0.002$; HET versus KO $P = 0.005$; PSD length WT versus KO $P = 0.007$; WT versus HET $P = 0.049$; HET versus KO $P = 0.399$; $n = 3$ brains for each genotype; WT synapse numbers: $n = 51$ for width and $n = 95$ for length, HET synapse numbers: $n = 70$ for width and $n = 99$ for length, KO synapse numbers: $n = 55$ for width and $n = 94$ for length; Kolmogorov–Smirnov test.)

synapses onto pyramidal cells by electron microscopy (EM) in adult knockout, heterozygous and wild-type animals (Fig. 3a). We observed that the cleft width was significantly larger in the heterozygotes versus wild types, and was further increased in the knockout mice (wild type, 14.37 ± 0.28 nm; heterozygote, 15.61 ± 0.28 nm; knockout, 17.37 ± 0.43 nm) (Fig. 3a, b), whereas the postsynaptic density (PSD) was shortest in the knockout and intermediate in heterozygotes compared to wild-type mice (Fig. 3a, b) (wild-type, 221.71 ± 7.34 nm, heterozygote, 195.45 ± 6.9 nm, knockout, 185.34 ± 6.67 nm). By contrast, excitatory (compared to inhibitory) synapses exhibited a significant but milder widening of the synaptic cleft in knockout versus wild-type mice (6.4% versus a 20.8% increase; Extended Data Fig. 5) and no difference in excitatory PSD length. Our results show that Cntnap4 joins the short list of molecules that contribute to the structural maturation of inhibitory interneuron synapses[3,4,17,18] and acts in a gene dose-dependent manner[19].

A number of synaptic molecules, including Cntnap2, have been extensively implicated in neuropsychiatric disorders. Given the synaptic localization of Cntnap4 and its differential effects on synaptic transmission in dopaminergic versus GABAergic neurons, it is a promising disease

target. Indeed, in addition to a handful of previously reported cases (see Extended Data Fig. 6a and Supplementary Information) our human genetics analysis identified 8 individuals with psychiatric illness and *CNTNAP4* gene disruption. Two harboured coding deletions, with one missing the whole gene, the other lacking the last 3 exons. The remaining six individuals had non-coding deletions, all contained within the 5′ region of intron II (Extended Data Figs 6–8 and Supplementary Information). Given these findings and the behavioural abnormalities described in *Cntnap2* mutant animals[1], we tested whether *Cntnap4* heterozygous or knockout mice exhibited abnormal behaviours consistent with neuropsychiatric disorders: grooming, pre-pulse inhibition (PPI), marble burying and behaviour in an open field arena (OFA) and an elevated plus maze (EPM).

Repetitive, perseverative movements comprise a common behavioural abnormality in individuals with autism spectrum disorders (ASDs) and manifest in mice as over-grooming[20,21]. Both knockout and heterozygous *Cntnap4* mice displayed a severe and highly penetrant over-grooming behaviour, resulting in whisker, face and sometimes body hair loss but rarely lesions (Fig. 4a). This was observed equally in male and female mice, and was apparent before weaning (Fig. 4b). It was even evident in wild-type offspring raised by mutant parents. By cross-fostering, we established unequivocally that allo-grooming in affected litters was always associated with the presence of a mutant *Cntnap4* allele (heterozygous or knockout) in one or both of the parents (Extended Data Fig. 9g). Strain differences also affected this behaviour, as line no. 13 did not display robust over-grooming when crossed onto an outbred background, but regained it when re-crossed into an inbred strain (Supplementary Information). Moreover, the observed over-grooming behaviour in mutant mice is unlikely to stem from overt changes in anxiety levels or deficits in locomotion, as OFA, EPM and marble burying tests did not reveal significant differences between the three genotypes (Extended Data Fig. 9a–f).

In addition to perseverative behaviours, neuropsychiatric patients often show impaired ability to process sensory information[22]. We performed PPI of the auditory startle reflex[22,23] and found that heterozygous and knockout mice exhibited both elevated startle responses and abnormal PPI indexes (Fig. 4c, d). On the basis of our cellular findings, we reasoned that the behavioural phenotypes might be reversed by augmenting inhibitory output and by dampening dopaminergic signalling.

There is extensive literature linking increased activity in the dopaminergic system and overt repetitive behaviours in both mice and humans[24,25]. We therefore administered the D2 receptor antagonist haloperidol via slow-release pellets (0.2 mg per kg or 0.6 mg per kg) implanted subcutaneously[26]. Haloperidol-treated parents showed a significant reduction in their own grooming score and did not over-groom their pups (Fig. 4f). In contrast, the pairs treated with vehicle did not show any overall hair and/or whisker recovery and continued to over-groom themselves and their offspring (Fig. 4f). After the 90-day treatment period when haloperidol levels were depleted, over-grooming progressively re-emerged (Fig. 4f, g). The effect of haloperidol on grooming was not the result of hypoactivity (Extended Data Fig. 10a). Therefore, increased dopaminergic signalling in mutant *Cntnap4* mice *in vivo* leads to over-grooming, a behaviour that can be rescued by chronic pharmacological treatment.

In order to assess if the defects in GABAergic transmission can account for the heightened startle or PPI defect in *Cntnap4* mutant animals, indiplon was administered. Indiplon is a highly specific positive allosteric modulator for $GABA_A$ receptors containing the α1 subunit[27,28], enriched in PV basket cells synapses[29]. Indeed, indiplon application *in vitro* (300 nM) enhanced spontaneous IPSCs recorded from layer 2/3 cortical pyramidal cells of *Cntnap4* mutant mice (Extended Data Fig. 10c). Acute administration of indiplon by oral gavage[27] restored the startle response in knockout and heterozygotes to wild-type levels (Fig. 4e). At the same dosage, wild-type animal startle was unaffected (Fig. 4e). Indiplon did not however affect PPI in knockout, heterozygote or wild-type animals (Extended Data Fig. 10b). This suggests that the GABAergic system is involved in the proper maturation of sensorymotor processing. Consistent with defective PV cell output, *Cntnap4* mutant mice exhibited mild epileptiform-like activity under deep anaesthesia that was not seen in controls (Extended Data Fig. 3b).

Our results show that Cntnap4 is located presynaptically and indicate that it functions in two distinct ways depending on the system. In dopaminergic synapses, which work by volume transmission on a relatively

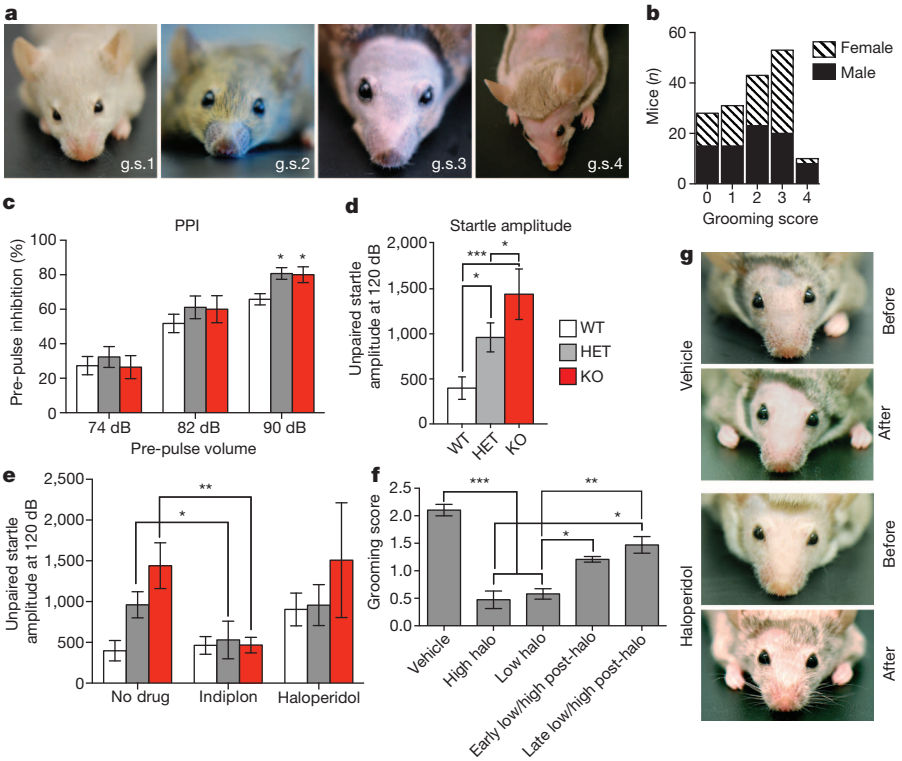

Figure 4 | Aberrant behaviour exhibited by *Cntnap4* mutant mice can be rescued by specific pharmacological intervention. **a**, Over-grooming score (g.s.) in *Cntnap4* mutant mice from 1–4 (1, lacks whiskers; 2, lacks whiskers and snout hair; 3, complete facial hair loss; 4, additional body hair loss). **b**, Grooming score for 165 *Cntnap4* mice. **c**, Increase in pre-pulse inhibition at 90 dB between mutant and wild type (WT, $n = 15$; HET, $n = 12$; KO, $n = 10$; WT versus HET, $P < 0.05$; WT versus KO, $P < 0.05$; one-way ANOVA, Tukey's post-hoc test). **d**, Increase in startle response amplitude in mutant versus wild type (WT, $n = 15$; HET, $n = 12$; KO, $n = 10$; WT versus HET, $P < 0.05$; WT versus KO, $P < 0.001$; HET versus KO, $P < 0.05$; one-way ANOVA, Tukey's post-hoc test). **e**, Startle amplitude in mutant mice was normalized upon acute administration of indiplon, but was unaffected by chronic delivery of haloperidol. **f**, Amelioration of over-grooming behaviour by chronic haloperidol (halo) administration. After the end of the haloperidol regimen, over-grooming returns. Early haloperidol treatment is 90 days after implantation; late haloperidol is 180 days after implantation (vehicle, $n = 58$ pups; high haloperidol, $n = 19$ pups; low haloperidol, $n = 44$; early post-haloperidol, $n = 24$ pups; late post-halo, $n = 17$ pups). **g**, Representative vehicle- and haloperidol-treated adult heterozygote before and after 60 days of haloperidol treatment. Re-emergence of facial hair and whiskers in treated mouse only.

slow timescale, mis-regulated release has a prominent role. In contrast, the GABAergic system works through fast synaptic transmission to deliver properly timed inhibition, and as a result the structural abnormality in the synapses predominates and leads to less efficient output with slower kinetics. Thus, in each instance, the kinetics of the system dictates the outcome of the loss of protein. Intriguingly, our findings that the loss of *Cntnap4* results in opposing failures in neurotransmission in the dopaminergic and GABAergic systems are consistent with the deficiencies observed in neuropsychiatric patients[5,30].

METHODS SUMMARY

Cntnap4 knock-in mice used in this study were generated by introducing enhanced GFP (eGFP) in frame with *Cntnap4* start codon. To characterize gene expression, eGFP was used to represent Cntnap4-expressing cells in the brain. Western blot analysis for Cntnap4 localization was performed on adult mouse cortex using a Cntnap4 rabbit polyclonal antibody described previously[8]. The Cntnap4–Fc fusion protein was applied to live neuronal cultures for *in vitro* localization studies. Evoked extracellular dopamine release was measured using fast-scan cyclic voltammetry of P60 *in vitro* slice preparations in wild type, heterozygous and knockout animals[11]. For paired cell recordings between FS and excitatory neurons, *Cntnap4* mice were crossed to a parvalbumin-cre:RFP reporter background to enable targeted physiological recordings. For synaptic ultrastructural analysis, P60 Cntnap4 wild type, heterozygous and knockout animals were analysed by electron microscopy, focusing on perisomatic inhibitory synaptic contacts. *Cntnap4* mice were assessed by a number of behavioural analyses including grooming score and pre-pulse inhibition[28,29] (San Diego Instruments). Pharmacological rescue was performed using indiplon (Tocris), which was administered acutely by oral gavage as well as haloperidol (Innovative Research of America), which was delivered chronically via subcutaneous slow-release pellet[27].

Online Content Methods, along with any additional Extended Data display items and Source Data, are available in the online version of the paper; references unique to these sections appear only in the online paper.

Received 14 January; accepted 11 March 2014.

Published online 25 May; corrected online 9 July 2014 (see full-text HTML version for details).

1. Peñagarikano, O. *et al.* Absence of CNTNAP2 leads to epilepsy, neuronal migration abnormalities, and core autism-related deficits. *Cell* **147,** 235–246 (2011).
2. Etherton, M. R., Blaiss, C. A., Powell, C. M. & Sudhof, T. C. Mouse neurexin-1alpha deletion causes correlated electrophysiological and behavioral changes consistent with cognitive impairments. *Proc. Natl Acad. Sci. USA* **106,** 17998–18003 (2009).
3. Fazzari, P. *et al.* Control of cortical GABA circuitry development by Nrg1 and ErbB4 signalling. *Nature* **464,** 1376–1380 (2010).
4. Berghuis, P. *et al.* Brain-derived neurotrophic factor controls functional differentiation and microcircuit formation of selectively isolated fast-spiking GABAergic interneurons. *Eur. J. Neurosci.* **20,** 1290–1306 (2004).
5. Lewis, D. A. Cortical circuit dysfunction and cognitive deficits in schizophrenia - implications for preemptive interventions. *Eur. J. Neurosci.* **35,** 1871–1878 (2012).
6. Blatt, G. J. & Fatemi, S. H. Alterations in GABAergic biomarkers in the autism brain: research findings and clinical implications. *Anat. Rec.* **294,** 1646–1652 (2011).
7. Ashrafi, S. *et al.* Neuronal Ig/Caspr recognition promotes the formation of axoaxonic synapses in mouse spinal cord. *Neuron* **81,** 120–129 (2014).
8. Spiegel, I., Salomon, D., Erne, B., Schaeren-Wiemers, N. & Peles, E. Caspr3 and Caspr4, two novel members of the Caspr family are expressed in the nervous system and interact with PDZ domains. *Mol. Cell. Neurosci.* **20,** 283–297 (2002).
9. Ho, A., Morishita, W., Hammer, R. E., Malenka, R. C. & Sudhof, T. C. A role for Mints in transmitter release: Mint 1 knockout mice exhibit impaired GABAergic synaptic transmission. *Proc. Natl Acad. Sci. USA* **100,** 1409–1414 (2003).
10. Atasoy, D. *et al.* Deletion of CASK in mice is lethal and impairs synaptic function. *Proc. Natl Acad. Sci. USA* **104,** 2525–2530 (2007).
11. Patel, J. C. & Rice, M. E. Monitoring axonal and somatodendritic dopamine release using fast-scan cyclic voltammetry in brain slices. *Methods Mol. Biol.* **964,** 243–273 (2013).
12. Li, X. *et al.* Enhanced striatal dopamine transmission and motor performance with LRRK2 overexpression in mice is eliminated by familial Parkinson's disease mutation G2019S. *J. Neurosci.* **30,** 1788–1797 (2010).
13. Doischer, D. *et al.* Postnatal differentiation of basket cells from slow to fast signaling devices. *J. Neurosci.* **28,** 12956–12968 (2008).
14. Hefft, S. & Jonas, P. Asynchronous GABA release generates long-lasting inhibition at a hippocampal interneuron-principal neuron synapse. *Nature Neurosci.* **8,** 1319–1328 (2005).
15. Labasque, M. & Faivre-Sarrailh, C. GPI-anchored proteins at the node of Ranvier. *FEBS Lett.* **584,** 1787–1792 (2010).
16. Krueger, D. D., Tuffy, L. P., Papadopoulos, T. & Brose, N. The role of neurexins and neuroligins in the formation, maturation, and function of vertebrate synapses. *Curr. Opin. Neurobiol.* **22,** 412–422 (2012).
17. Chang, M. C. *et al.* Narp regulates homeostatic scaling of excitatory synapses on parvalbumin-expressing interneurons. *Nature Neurosci.* **13,** 1090–1097 (2010).
18. Sylwestrak, E. L. & Ghosh, A. Elfn1 regulates target-specific release probability at CA1-interneuron synapses. *Science* **338,** 536–540 (2012).
19. Cathala, L., Holderith, N. B., Nusser, Z., DiGregorio, D. A. & Cull-Candy, S. G. Changes in synaptic structure underlie the developmental speeding of AMPA receptor-mediated EPSCs. *Nature Neurosci.* **8,** 1310–1318 (2005).
20. Peça, J. *et al. Shank3* mutant mice display autistic-like behaviours and striatal dysfunction. *Nature* **472,** 437–442 (2011).
21. Chao, H. T. *et al.* Dysfunction in GABA signalling mediates autism-like stereotypies and Rett syndrome phenotypes. *Nature* **468,** 263–269 (2010).
22. Geyer, M. A., Krebs-Thomson, K., Braff, D. L. & Swerdlow, N. R. Pharmacological studies of prepulse inhibition models of sensorimotor gating deficits in schizophrenia: a decade in review. *Psychopharmacol.* **156,** 117–154 (2001).
23. Stark, K. L., Burt, R. A., Gogos, J. A. & Karayiorgou, M. Analysis of prepulse inhibition in mouse lines overexpressing 22q11.2 orthologues. *Int. J. Neuropsychopharmacol.* **12,** 983–989 (2009).
24. Champagne, F. A. *et al.* Variations in nucleus accumbens dopamine associated with individual differences in maternal behavior in the rat. *J. Neurosci.* **24,** 4113–4123 (2004).
25. Grados, M. A. The genetics of obsessive-compulsive disorder and Tourette's syndrome: what are the common factors? *Curr. Psychiatry Rep.* **11,** 162–166 (2009).
26. Crowley, J. J. *et al.* Antipsychotic-induced vacuous chewing movements and extrapyramidal side effects are highly heritable in mice. *Pharmacogenomics J.* **12,** 147–155 (2012).
27. Foster, A. C. *et al. In vivo* pharmacological characterization of indiplon, a novel pyrazolopyrimidine sedative-hypnotic. *J. Pharmacol. Exp. Ther.* **311,** 547–559 (2004).
28. Petroski, R. E. *et al.* Indiplon is a high-affinity positive allosteric modulator with selectivity for alpha1 subunit-containing $GABA_A$ receptors. *J. Pharmacol. Exp. Ther.* **317,** 369–377 (2006).
29. Klausberger, T., Roberts, J. D. B. & Somogyi, P. Cell type- and input-specific differences in the number and subtypes of synaptic $GABA_A$ receptors in the hippocampus. *J. Neurosci.* **22,** 2513–2521 (2002).
30. Castellanos, F. X. *et al.* Sensorimotor gating in boys with Tourette's syndrome and ADHD: preliminary results. *Biol. Psychiatry* **39,** 33–41 (1996).

Supplementary Information is available in the online version of the paper.

Acknowledgements The authors are grateful to R. Froemke for critically reading the manuscript, to B. Benedetti, M. McKenzie Chang, L. Cobbs, B. A. Heller, T. Petros and N. Yumoto (all NYU) for help with experiments and analysis and to Charles Nicholson (NYU) for providing specialized software to analyse *V*max. Research in the Fishell laboratory is supported by the NIH (grants R01 NS081297, R01 MH071679, R01 NS074972, P01 NS074972 to B.R. and G.F.) and the Simons Foundation (94534). The Rice laboratory is supported by the NIH (grants R01 NS036362 and R01 DA033811) and the Attilio and Olympia Ricciardi Research Fund. The Rudy laboratory is supported by the NIH (NS30989). The Peles laboratory is supported by the NIH (grant NS50220) and the Israel Science Foundation. T.K. support was provided through postdoctoral fellowships from the Patterson Trust and Roche. E.A. support was provided by New York State through its NYSTEM initiative (C024326) and fellowship from Canadian Institutes of Health Research. J.C.P support was provided by NYU COE Addiction Seed Grant. This work was funded by the Institut Pasteur, INSERM, AP-HP, University Paris Diderot and the Bettencourt-Schueller, Orange, FondaMental, Conny-Maeva, Cognacq-Jay foundations.

Author Contributions T.K., E.A. and G.F. designed the study and wrote the manuscript. T.K. and E.A. performed all the experiments and analysis except for the following: J.C.P. performed the *in vitro* voltammetry experiments and analysed the data. I.K. performed the majority of the *in vitro* paired recordings. M.K., L.R.-M. and S.M. provided the SNP data. J.G. and H.H. provided the intronic CNV data. D.H., B.K., G.H., R.D. and T.B. provided the exonic CNV data. S.R. performed the synaptosome preparation and western blots. D.S. and E.P. made the *Cntnap4* mouse. A.G. performed the verification of the *Cntnap4* mouse. N.C.R. performed the *in vivo* electrophysiological experiments. C.H. set up and advised on behavioural experiments. J.A.G., R.W.T., B.R. and M.E.R. advised on experiments and manuscript preparation.

Author Information Reprints and permissions information is available at www.nature.com/reprints. The authors declare no competing financial interests. Readers are welcome to comment on the online version of the paper. Correspondence and requests for materials should be addressed to G.F. (gordon.fishell@med.nyu.edu).

METHODS

Human genetics

CNV identification. The subjects included in this study that have been reported in previously published work have given their consent[31–33]. In the case of the new cohort of 784 patients with ASD, it was approved by the local Institutional Review Board (IRB) and written informed consents were obtained from all participants of the study. The local IRB are the Comité de Protection des Personnes (Île-de-France Hôpital Pitié-Salpêtrière Paris, France). Written informed consent was obtained from all participating subjects. As proband of family II was under 18 years old, the proband's consent and written parental consent were obtained.

Genome-wide SNP genotyping for ASDs[31] and ADHD[32] cases and controls was done using the InfiniumII HumanHap550 BeadChip (Illumina) at the Center for Applied Genomics at the CHOP and with the Illumina Infinium 1M array at the Centre for National Genotyping (CNG, Evry, France). Schizophrenia[33] samples were genotyped using the Affymetrix 6.0 array. To identify copy-number variations (CNVs), we used PennCNV and QuantiSNP. Quality metrics for inclusion included: identification rate $>$ 98%, standard deviation of the normalized intensity (LRR) $<$ 0.35, European descent based on principle components analysis, low genomic inflation factor between case and control populations, (GC base pair wave factor) $<$ 0.05, CNV call count $<$ 70 and no duplicate samples. Statistical association was assessed using Fisher's exact test.

CNV validation. TaqMan copy number assay experiments were run on Applied Biosystems 7900HT Fast Real-Time PCR System to validate the presence of deletions on *CNTNAP4*. Applied Biosystems CopyCaller Software performed relative quantitation analysis of genomic DNA targets using the real-time PCR data from TaqMan Copy Number Assay experiments or the Universal Probe Library (UPL) system from Roche. HS05422219_cn assayed Chr16:74920706 (hg18) on the CHOP deletion overlapping region. Each assay was conducted with 2–3 replicates for target region probe-set and control region probe-set. All deletions predicted by the Illumina array data were positively validated. To test if the deletion extended across the upstream exon 2 of *CNTNAP4* which was not definitive based on the Illumina probe resolution, HS02779798_cn assayed Chr16:74907734 (hg18) just upstream of *CNTNAP4* exon 2. All samples showed diploid signals indicating that exon 2 was not overlapped by the deletions. Positive and negative controls were used to confirm probe accuracy.

SNP analysis. A sample of 232 individuals meeting diagnostic criteria for schizophrenia or schizo-affective disorder and their families were genotyped on a Human Genome-Wide SNP Array 5.0 (Affymetrix), which contains 500,568 SNPs (manuscript in preparation). Among the available data, we extracted information on 1,045 genotyped and imputed SNPs spanning the *CNTNAP4* locus and 500 bp on either end of the gene. The sample has been previously described in detail[34–37]. Average call rate on arrays used in this study was 99.43%. All microarray experiments were performed in the Vanderbilt Microarray Shared Resource. Quality control procedures per family, individual, and marker were performed with PLINK (http://pngu.mgh.harvard.edu/purcell/plink/)[38] and PedStats (http://www.sph.umich.edu/csg/abecasis/PedStats/). Following quality control we selected samples with a call rate $>$ 95%. We eliminated from the analysis duplicated SNPs, monomorphic SNPs and SNPs with a Hardy–Weinberg exact test $P < 10^{-6}$. Only SNPs with minor allele frequency $>$ 0.01 were included in the downstream analyses. We also checked for Mendelian inheritance errors among families and removed SNPs with $>$4 Mendelian errors in the total sample. Imputation of non-genotyped HapMap SNPs was performed with MACH (http://www.sph.umich.edu/csg/abecasis/MACH/) using 100 MarKOv iterations with the two-step procedure recommended in the manual. HapMap Phased Haplotypes (release 22) on CEU subjects were used in the imputation. After imputation, only SNPs with a MACH $R^2 > 0.3$ were considered further. This estimates the correlation between imputed and true genotypes; a value less than 0.3 flags poorly imputed SNPs[39]. In addition, Mendelian checks and Hardy–Weinberg equilibrium tests were performed to eliminate unreliable imputation calls in order to include imputed genotypes in downstream analyses. Imputed SNPs were then analysed similarly to the genotyped SNPs. Family-based association tests for single SNPs were performed using LAMP (http://www.sph.umich.edu/csg/abecasis/LAMP/). LAMP assesses association by taking into account linkage information from the pedigrees and the multiple generations in the pedigrees and appropriately corrects for family structure[40,41]. We adopted a free model for the analysis that does not constrain the penetrance for the three genotypes.

Generation of mutant mice. The *Cntnap4* targeting vector was designed to replace a genomic fragment of 585 bp containing the first exon of the gene, encoding the ATG and the signal sequence, with an in frame *egfp*, followed by an oppositely directed *neo* gene (Fig. 1b). A 2.45 kb genomic fragment located upstream of exon 1 was amplified by PCR from 129SvJ genomic BAC library using primers 5′-GACAGTCTTAAATAGCCTAGAATC-3′ and 5′-CTCCAGCGCTCTGAGAGCCA-3′ and cloned into pKO-901 Scrambler vector (Lexicon Genetics) containing GFP. A 6.6 kb fragment downstream of exon 1 was amplified using the primers 5′-GACATACTGCAGACTTCGCGG-3′ and 5′-CATGCACCATGTATGCGCAGGA-3′ and cloned into the same plasmid, followed by the insertion of a neomycin selection cassette between the two homology arms. A promoter-driven diphtheria toxin A fragment (DT) that was then added and used to select against random integration. This targeting vector resulted in a deletion of 585 bp R1 ES cells were electroporated with the linearized targeting construct, and recombinant ES clones were selected with G418. Clones containing correctly targeted integrations were identified by Southern blot analysis of EcoRI-digested genomic DNA using a probe (prepared by PCR using primers 5′-CATGTATAAGCTCTCTCCTTCCG-3′ and 5′-CTGACAGCACAGHGCCCAGACC-3′) located outside of the targeting vector sequence. Correctly targeted ES cell lines were used to produce chimaeric mice by aggregation, as previously described[42]. Chimaeric mice were mated with ICR females, and germline transmission was detected by coat colour and Southern analysis of tail DNA. Genotyping of progenies was performed by PCR of genomic tail DNA using the primer sets described in Fig. 1a; *a* (within the first intron) ACACTACTTAAGCGGGTGGTG; *b* (within exon 1) GGATCTGTCGCTGGAGCTG; and *c* (within the neo gene) CCTCTGAGCCCAGAAAGCG. Two lines were generated (designated no. 13 and no. 145) from two different ES clones. These lines were backcrossed once (no. 149) or five times (no. 13) to ICR and then kept intercrossed. Most of the data presented was obtained using knockout line no. 149. All experiments were performed in compliance with the relevant laws and institutional guidelines and were approved by the Animal Care and Use Committees of NYU and the Weizmann Institute.

RNA analysis. Total RNA was isolated from freshly dissected tissues using either TRI-reagent (Sigma-Aldrich) and cDNAs were obtained with SuperScript-II reverse transcriptase (Invitrogen) using oligo-dT. The following specific PCR primer sets were used for RT–PCR analysis: actin, 5′-GAGCACCCTGTGCTGCTCACCGAGG-3′ and 5′-GTGGTGGTGAAGCTGTAGCCACGCT-3′; *Cntnap4* (exons 1–3), 5′-GGATCTGTCGCTGGAGCTG-3′ and 5′-CCACTATCACTGAACATCAGG-3′; *Cntnap4* (exons 2–4), 5′-GGTCCCCACTTGTGTCCAAC-3′ and 5′-TACAACCACCGGTATGCAC-3′.

Antibodies and western blot analysis. Brains were homogenized in 20 mM HEPES pH 7.4, 0.32 M sucrose, 1 mM EGTA, 1.5 mM $MgSO_4$, protease inhibitors (Sigma P8340) centrifuged at low speed (1,000*g*) for 10 min. Supernatants were collected and centrifuged at high speed (20,000*g*) for 1 h. Pellets were then solubilized in 2% NP-40, 2 mM $MgCl_2$, protease inhibitors (Sigma P8340) in PBS, incubated on ice for 15 min and centrifuged at high speed (20,000*g*) for 15 min. SDS–PAGE and western blotting was carried out as previously described[43] with the exception that the chemiluminescence signal was detected using the ChemiDoc MP System (Bio-Rad). Affinity purified antibodies against Cntnap4 (rabbit (rb) 1:500) were generated as described previously using a GST–Cntnap4CT (CT, carboxyl terminus) Sepharose[44].

To quantify postsynaptic $GABA_A$ receptors and other synaptically localized proteins, the following antibodies were employed: $GABA_A$-α1 (NeuroMab, mouse (ms) 1:1,000); $GABA_A$-γ2 (PhosphoSolutions, rb 1:1,000); N-cadherin (BD Pharmingen, ms 1:1000); PSD-95 (NeuroMab, ms 1:1,000); gephyrin (Synaptic Systems, ms 1:1,000). Blots were visualized using IRDye secondary antibodies (Li-Cor, 1:30,000), scanned and quantified using the Li-Cor Odyssey system.

Presynaptic and postsynaptic fractionation. Synaptosomal fractions from mouse brain were prepared as described previously[45]. Presynaptic and postsynaptic fractions were prepared from synaptosomes by extraction at differential buffer pH as described previously[46,47]. Equal amount of fractions (20 μg) were loaded onto an SDS–PAGE gel. Western blots were probed with different antibodies. Synaptophysin was used as loading control for WB, P2, whole synaptosome, and presynaptic fractions. PSD-95 was used as a loading control for postsynaptic fractions.

***In vitro* voltammetric dopamine recordings.** Coronal striatal slices (350-μm thick) were prepared from male littermate *Cntnap4*$^{+/+}$, *Cntnap*$^{-/+}$ and *Cntnap4*$^{-/-}$ mice (3 to 4 months old, 4 mice per genotype, 2 slices per mouse) using a VT1200S vibrating blade microtome (Leica Microsystems) and allowed to recover for at least an hour at room temperature as described previously[48,49]. To decrease any bias in dopamine recordings, we examined 2 mice per experimental day using a design in which each mouse genotype was assessed either first or second on the experimental day and paired with one of each of the other genotypes.

For recording, slices were transferred to a submersion chamber (Warner Instruments) maintained at 32 °C and superfused at 1.2 ml min^{-1} with bicarbonate-buffered aCSF containing (in mM): NaCl (124); KCl (3.7); $NaHCO_3$ (26); $MgSO_4$ (1.3); KH_2PO_4 (1.3); glucose (10); $CaCl_2$ (2.4), and saturated with 95% O_2/5% CO_2. After a brief equilibration period of 30 min, fast-scan cyclic voltammetry with carbon fibre electrodes was used to monitor $[DA]_o$ evoked by local electrical stimulation (0.1 ms pulse duration, 0.4 mA amplitude) CPu and NAc core, as described previously[48,49]. Carbon-fibre electrodes (30–70 μm length) were constructed in-house using a 7 μm diameter carbon fibre (Goodfellows) according to methods described by Patel and Rice[18]. Fast-scan cyclic voltammetry measurements were made using a Millar voltammeter (available by special request to Dr. Julian Millar at St. Bartholomew's and the Royal London School of Medicine and Dentistry, University of London,

UK). The scan range used was −0.7 V to +1.3 V (versus Ag/AgCl), scan rate was 800 V s^{-1}, and the sampling interval was 100 ms. The experimental design for each slice involved sampling $[DA]_o$, evoked by a single pulse or by a brief pulse train of 20 pulses at 10 Hz in 8 recording sites (4 sites for each stimulation parameter), within the dorsolateral CPu and 8 recording sites in the NAc core. Given that 2 slices were examined per mouse, this gave a total n number of 8 recordings for each stimulation parameter per region in each mouse. A frequency response curve (5 pulses, 5, 10, 25, 50 and 100 Hz) was also collected for each region in each slice[49].

Identification of released dopamine was based on voltammograms with single oxidation and reduction peak potentials that define the voltammetric signature of dopamine[48]. Evoked $[DA]_o$ was quantified by postexperimental calibration of carbon-fibre electrodes with known concentrations of dopamine at 32 °C[48]. To quantify changes in dopamine uptake by the DAT, we fitted the initial segment of the falling phase of single-pulse evoked $[DA]_o$ curves to the Michaelis–Menten equation to extract V_{max} (the maximal rate constant for uptake which is proportional to the number of functional DATs) values (for details see refs 50, 51). The value of K_m (which is inversely related to the affinity of the DAT for dopamine) was fixed at 0.9 μM[50,51] and assumed not to be altered in the transgenic lines. The use of single pulses for this analysis allows evoked $[DA]_o$ to be assessed in the absence of autoreceptor regulation by endogenous dopamine and avoids modulation by concurrently released glutamate or GABA[48,52].

***In vitro* electrophysiology**

Acute slice preparation. Mice of postnatal day 17–22 or 60–90 were anesthetized and decapitated, and their brains quickly removed and placed into ice-cold high-sucrose artificial CSF (ACSF) (composition in mM: 85 NaCl, 25 $NaHCO_3$, 2.5 KCl, 1.25 NaH_2PO_4, 0.5 $CaCl_2$, 7 $MgCl_2$, 10 glucose, 75 sucrose) saturated with 95% O_2, 5% CO_2, at pH ~7.3. Using a vibratome (VT 1000S; Leica Microsystems or Vibratome), coronal sections (250–300 μm) were cut containing the somatosensory barrel field cortex. The slices were allowed to recover in recording ACSF (same as above but 130 NaCl, 2 $CaCl_2$, 2 $MgCl_2$, 0 sucrose) at room temperature for at least 45 min before recording. Acute slices were then placed in a recording chamber mounted on the stage of an upright microscope (Axioscope; Zeiss) equipped with immersion differential interference contrast objectives (×5, ×40) coupled to an infrared camera system (Zeiss), superfused at a rate of 1–2 ml min^{-1} with oxygenated recording ACSF, and maintained at a temperature of 31 ± 1 °C.

Electrophysiological recordings and data analysis. Experiments were performed in current-clamp mode using the Axoclamp 2B (Molecular Devices) or the Axopatch 200B amplifier and in voltage clamp using the latter.

When recording in current-clamp mode for assessing the active and passive membrane properties, cells were patched with electrodes containing the following (in mM): 126 K-gluconate, 10 HEPES, 10 Na2-phosphocreatine, 4 KCl, 4 Mg-ATP, 0.3 Na-GTP, pH 7.3, with KOH; the osmolarity was ~280 mOsmol. A series of sub- and supra-threshold current steps were applied and the analysis was done in Clampfit. The resting membrane potential (V_{rest}) was ascertained in current clamp right after rupturing the patch by applying zero current.

Spontaneous synaptic currents were recorded using a pipette filled with 40 mM KCl and 90 mM K-gluconate with the rest being the same as for current clamp recordings (see above). The rationale for using such a concentration of KCl was to try to differentially amplify the proximally occurring spontaneous IPSCs (sIPSCs) such as the ones coming from PV basket cells compared to all other IPSCs. The currents were filtered online at 3 kHz and recorded with a sampling rate of 10 kHz for at least 120 s. The series resistance was compensated online by 50%. No correction was made for the junction potential between the pipette and the ACSF. Individually acquired sIPSCs were recorded at $V_H = -65$ mV after application of kynurenic acid (3 mM) or a combination of CNQX (20 μM) and D-AP5 (20 μM). The recorded files were analysed using Minianalysis software (Synaptosoft, Decatur, GA, USA). The synaptic values were obtained for the average trace after visual inspection of individual events. The decay time was calculated by fitting the average trace with a single exponential. For generating the cumulative distribution plots and performing the K–S statistics all the individual events were taken for all the cells recorded in each group and were compared against each other.

For paired-cell recordings the recording pipettes were filled with the following (in mM): 88 KCl, 42 K-gluconate, 10 HEPES, 10 Na2-phosphocreatine, 4 Mg-ATP, 0.3 Na-GTP, pH 7.3 with KOH, to increase the driving force for Cl^- ions ($E_{Cl} = -11$ mV) to the extent that the IPSC polarity was inward at the holding potential (V_H) of −80 mV. Biocytin was added to the intracellular solutions before recording at a final concentration of 0.1–0.5% (w/v). Recording electrodes had resistances between 4 and 6 MΩ. Access resistance was always monitored to ensure the stability of recording conditions. Cells were only accepted for analysis if the initial series resistance was ≤ 20 MΩ and did not change by >20% throughout the recording period. No correction was made for the junction potential between the pipette and the ACSF, and therefore the recorded membrane potential, as calculated post hoc using a junction potential calculator, was 11 mV more depolarized than the true membrane potential for high-Cl^- intracellular solution. The presynaptic cells were held at −70 mV and the postsynaptic neurons were voltage clamped at the same potential, but during the occurrence of presynaptic action potentials a voltage pulse was applied that hyperpolarized the cell to −80 mV to obtain unitary IPSCs. Postsynaptic currents were filtered at 3 kHz and recorded with a sampling rate of 20 kHz. They analysis of the synaptic events was performed in Clampfit.

All values presented in the manuscript are average ± standard error of the mean (s.e.m.) and all the statistical values are obtained doing a standard Student's t-test, a Mann–Whitney or a Kolmogorov–Smirnov test (*$P \leq 0.05$, **$P \leq 0.01$, ***$P \leq 0.001$).

***In vivo* electrophysiology.** Wild type, heterozygous and homozygous adult *Cntnap4* mutant mice were anaesthetized with ketamine/xylazine (100 mg per kg ketamine, 20 mg per kg xylazine, i.p.). A maintenance injection (10 mg per kg ketamine, 2 mg per kg xylazine) was given every 30 min. Depth of anaesthesia was verified periodically throughout the experiment by absence of the foot withdrawal reflex. Mice were placed in a sterotaxic frame and secured in place with ear bars (David Kopf Instruments). Body temperature was maintained at 37 °C ± 1 °C using an electric heating blanket. An incision was made along the midline of the scalp to expose the skull and a craniotomy 1 mm in diameter was made with a dental drill over primary somatosensory cortex (approximately 1 mm posterior and 3 mm lateral to bregma). A well was made around the craniotomy with QwikSil, and the exposed brain was kept moist by application of normal saline. A small hole was made in the dura and a 32-channel silicon probe (a linear array of 32 contacts, 50 μm apart) was positioned normal to the cortical surface with the most superficial contact just above the surface of the brain. An hour after positioning the probe, a series of 1-min recordings was made every 2–5 min. Maintenance doses were discontinued for 30–60 min, until the LFP exhibited a reduction in the amplitude of the slow oscillation, at which point a large dose of ketamine/xylazine (150 mg per kg ketamine, 30 mg per kg xylazine) was given. Data acquisition and analysis was performed using custom routines written in Igor Pro (Wavemetrics). LFPs for analysis were obtained by subtracting the signal from the most superficial recording site from the signal from a site 600–700 μm deep. Field spikes were defined as negative deflections in the LFP greater than three standard deviations in amplitude.

Immunohistochemistry. Mice were trans-cardially perfused with 4% ice-cold paraformaldehyde (PFA), the brain was removed from the skull and immersed in 4% PFA for an hour. It was then washed at least 3 times for 5 min each and subsequently immersed in 25% PBS sucrose solution overnight. The following day it was mounted in OCT and 12-μm sections were cut using a cryostat and collected on glass slides. After blocking with 10% donkey serum in 0.3% Triton PBS for an hour at room temperature (RT), slices were incubated with primary antibodies at 4 °C overnight. The following day the slices were washed at least three times for 10 min each in PBS and then incubated with the secondary antibody for 1 h at RT. The slices were then washed a few times and mounted in Fluoromount-G for visualization under an epifluorescent microscope (Zeiss AxiosKOp using Spot Advanced software) or under a confocal microscope (Zeiss LSM 510 Meta system).

The molecular expression profiles and layering of Cntnap4-positive interneurons was analysed on somatosensory barrel cortex slices at P21, P30 and P60 brains from *Cntnap4* wild type, *Cntnap4* heterozygous and knockout littermate mice, which were counterstained with DAPI.

The following antibodies were used at specific concentrations: rabbit anti-GFP (1:20,00; Invitrogen), rat anti-GFP (1:2,000; Nacalai Tesque), goat anti-GFP (1:2,000; Rockland), mouse anti-parvalbumin (1:1,000; Sigma), guinea pig anti-parvalbumin (1:1000; a gift from Dr. D.A. Lewis, University of Pittsburgh) rat anti-somatostatin (1:500; Millipore Bioscience Research Reagents), rat anti-somatostatin (1:250; Chemicon), rabbit anti-neuropeptide Y (1:500; ImmunoStar), rabbit anti-vasoactive intestinal polypeptide (1:500; ImmunoStar), mouse anti-calretinin (CR) (1:1,500; Millipore Bioscience Research Reagents), rabbit anti-calretinin (1:1,500; Millipore Bioscience Research Reagents), mouse anti-reelin (CR50) (1:500; MBL). Secondary antibodies conjugated with Alexa Fluor dyes 488, 594 or 643 (Invitrogen) or AMCA (Jackson Immunoresearch) raised from the same host used for blocking serum were chosen for signal visualization. Fluorescent images were captured using a cooled-CCD camera (Princeton Scientific Instruments) using MetaMorph software (Universal Imaging).

Double *in situ* hybridization. Sections were dried for 1 h before 10 min fixation in 4% PFA. After wash, endogenous peroxidase activity was quenched by 1.5% H_2O_2 in methanol for 15 min at room temperature. Sections were then treated in 0.2 M HCl for 8 min before a proteinase K treatment (10 μg ml^{-1}; Roche) for 3 min and a post-fixation in 4% PFA for 10 min at 4 °C with washing steps in between. Before hybridization, the tissue was acetylated in TEA (tetraethylammonium) (0.185 g ml^{-1}; Sigma-Aldrich), 0.5N NaOH, and 0.25% acetic anhydride (Sigma-Aldrich). The digoxigenin (DIG)- and FITC-labelled probes (full-length cDNA probes of *Gad67*, *Cntnap4* (ref. 44) were mixed 2 μl per slide in 250 μl of hybridization buffer (50% formamide, 10% dextrane sulphate, 0.25 mg ml^{-1} yeast RNA, 0.3 M NaCl, 20 mM Tris, 5 mM EDTA, 10 mM $NaPO_4$, and 1% N-lauroylsarcosine in Denhardt's solution)

and denatured at 80 °C for 2 min. Hybridization was carried out overnight at 55 °C. After hybridization, the sections was rinsed in a 2× SSC with 50% formamide solution for 30 min at 65 °C before several washes in RNase buffer (0.5 M NaCl, 10 mM Tris, pH 7.5, and 5 mM EDTA, pH 8.0). The tissue was treated with RNase (20 μg ml^{-1}; Roche) in RNase buffer for 30 min at 37 °C before rinsing in decreasing amounts of SSC (2×, 0.2×, and 0.1×) for 15 min at 37 °C each. After equilibrating in TN buffer (0.1 M Tris, pH 7.5, and 0.15 M NaCl), the sections were blocked in 0.5% blocking reagent (Roche) in TN buffer for 30 min at room temperature. The sections were then incubated with primary antibody against FITC or DIG overnight at 4 °C. On the third day, sections were rinsed in TNT buffer (TN buffer with 0.05% Tween 20) before amplification and visualization step using the TSA Plus Cyanine 3/Fluorescein System (PerkinElmer) according to the manufacturer's instructions (10–60 min incubation). After washes in TNT, the peroxidase was quenched in 3% H_2O_2 in TN for 2 h at room temperature before incubation with the other primary antibody for 1 h at room temperature followed by visualization using the same kit as above. After washes in TNT, sections were incubated in DAPI before mounting in Fluoromount-G. Images were obtained using a confocal microscope (Zeiss LSM 510 Meta system).

Hippocampal cultures. Cultures were prepared from embryonic day 19 Sprague Dawley rat embryonic brain tissue. Animals were killed by CO_2 in compliance with New York University Medical Center's Institutional Animal Care and Use Committee. Hippocampal neurons were prepared as described previously[53]. Neurons were plated at a density of 100,000 cells on poly-L-lysine-coated glass coverslips in a six-well plate for immunofluorescence. Neurons were grown in Neurobasal medium with B27 (Invitrogen). At the first change of medium, a one-time dose of the drug AraC (4 μM; Sigma-Aldrich) was added to inhibit growth of dividing cells for immunofluorescence experiments[54]. All immunocytochemical reactions were performed on five-week-old cultures.

To identify localization of Cntnap4 binding, a tagged-Cntnap Fc protein was applied in the cultures as described previously[55]. Briefly, live cells are washed with binding buffer, incubated with 100 nM control human Fc or Cntnap4–Fc for 90 min at room temperature, rinsed five times and then fixed with 4% PFA in PBS. After rinsing with HEPES buffer, endogenous alkaline phosphatase (AP) activity was inactivated by heating at 65 °C for 30 min. An AP-conjugated antibody was applied to visualize signal. For experiments in which cells were double-labelled with gephyrin, cells were permeabilized after fixation, AP heat inactivation was not performed. Mouse anti-gephyrin (1:250; Synaptic Systems) was then applied applied and anti-human Alexa 488-conjugated secondary and anti-mouse Alexa 594 were used to visualize signal.

Transmission electron microscopy:. The mice were aneasthetized and were perfused transcardially with saline followed by fixative containing 4% paraformaldehyde (PFA) and 2.5% glutaraldehyde in 0.1 M phosphate buffer (PB, pH 7.4). Brains were sliced using a brain slicer so as to obtain only parts of the somatosensory barrel field cortex. The cut pieces were then post-fixed with the same fixative at room temperature for 2 h and then at 4 °C overnight. After washing with PB 3 times for 15 min, the samples were fixed in 1% OsO_4 for 2 h, block stained with 1% uranyl acetate for 1 h, dehydrated in ethanol and embedded in EMbed 812 (Electron Microscopy Sciences, Hatfield, PA). Then 60-nm ultrathin sections were cut and stained with uranyl acetate and lead citrate by standard methods. Stained grids were examined under a Philips CM-12 electron microscope (FEI; Eindhoven, The Netherlands) and photographed with a Gatan (4k × 2.7k) digital camera (Gatan, Pleasanton, CA). For analysing perisomatic inhibitory synapses, we first identified pyramidal cells based on their characteristic body shape from which an apical dendrite emanated towards the pia. The soma was surveyed under high magnification and symmetric synapses were identified as appositions between terminals containing vesicles and most of the times mitochondria and soma membrane bearing a very narrow post-synaptic density (PSD). The synaptic cleft was measured as the gap between the presynaptic and postsynaptic membranes under digitally zoomed-in images and the synaptic length as the length of the PSD. For excitatory synapses randomly selected assymetric contacts were captured against unidentified elements and the synaptic cleft and PSD length were analysed similarly to the inhibitory synapses and as previously reported. The analysis was performed in ImageJ (NIH). Although it was not originally done blind by the authors, an independent individual not part of the study assessed half of the data set blindly and verified the original findings.

Only synapses with a clear post- and presynaptic element were included in the analysis for synaptic length. Only synapses that had a clear synaptic cleft separating the pre- and post-synaptic elements were taken for width measurements.

Behavioural testing. The behavioural testing was done in the following order: OFA-EPM-PPI in 3–4 cohorts of mice.

Open field analysis (OFA). OFA was measured in an activity test chamber (27.3 cm × 27.3 cm) in a self-enclosed sound attenuating cubicle (Med Associates, St. Albans, VT) with 16 infrared light beams per side. Mice were released into the centre of the OFA for testing. The activity of the mouse over 10 or 15 min was determined by beam breaks and recorded by computer for subsequent analysis. The apparatus was thoroughly cleaned with 70% isopropanol before each mouse was tested. The periphery and centre were arbitrarily defined (6 cm in 27.3 cm) and the dependent variables measured were distance travelled, time in the periphery versus time in centre and vertical time. Illumination levels during testing were maintained at a constant 60 lx.

Elevated plus maze (EPM). The EPM consisted of four white, equally spaced arms, 39 cm in height and 33.9 cm from the centre of the apparatus. Two opposing arms were each enclosed by white walls extending 15.3 cm above the surface and two arms were open. Individual mice were placed in the centre of the maze to start and their activity recorded on computer for 5 min by video camera (Bosch LTC 0335). Animals were released using bottomless holding chamber at the start of the test. The animals' movements were captured and analysed with Ethovision XT software (Noldus, Wageningen, Netherlands). The apparatus was thoroughly cleaned with 70% isopropanol before each mouse was tested. Dependent variables were distance covered and time spent in the exposed versus enclosed arms and centre. Illumination levels during testing were maintained at a constant 195 lx.

Pre-pulse inhibition. PPI was determined using SR Lab startle response chambers (San Diego Instruments, San Diego, CA, USA). Each mouse was placed into a Plexiglas cylinder attached to a piezoelectric sensor. The startle response to an acoustic stimulus was measured in the presence of a 65 dB white noise background that began a 5-min acclimation period. Each session consisted of a randomized block design of 40 trials that presented a 20 ms pre-pulse of 74, 82 or 90 dB followed 100 ms later by either a 40 ms 120 dB startle pulse or no pulse at all (null). The ITI averaged 15 s but was pseudo-randomized during presentations. The apparatus was thoroughly cleaned with 70% isopropanol before each mouse was tested. The percent PPI for each pre-pulse startle stimulus was determined by dividing the startle response to a pre-pulse stimulus by the startle response for that trial, multiplying the quotient by 100 and subtracting the product from 100 (100 − (pre-pulse startle response/startle response) × 100) for each trial. The mean response for each group, wild type, heterozygous and knockout mice was calculated for each pre-pulse stimulus level. For the indiplon experiments, the drug was orally gavaged at a concentration of 10 mg per kg 30 min to 1 h before performing the PPI test, as that is when the drug reaches its peak concentration in the brain[56].

Animals were excluded from the analysis when non-responsive to the acoustic stimulus, presumed to have hearing deficits.

Grooming. Mice were scored on a scale from 1–4 depending on the extent of their grooming. A score of 0.5 means that the whiskers were half the length of controls, whereas 1 means that they were trimmed all the way to the skin. A score of 2 indicates that the hair around whiskers was also gone, 3 that there was a more extensive and spread facial hair loss and 4 indicates additional body hair loss. For the pharmacological rescue of the overgrooming phenotype, custom-made slow release pellets lasting for 90 days were used (Innovative Research of America, Sarasota, Florida) and placed subcutaneously using a 10 gauge precision trochar in wild-type and heterozygous mice under 5 min of isoflurane anaesthesia.

Marble burying. Mice were placed in the middle of a cage (27 × 16.5 × 12.5 cm) with 5 cm high corncob bedding that had 20 black marbles of ~14 mm diameter gently placed in a 4 × 5 arrangement as previously reported[57,58]. One picture was taken before putting the mice in the cage and another after taking the mice out of the cage. The mice were video-monitored for 10 min and the extent of marble burying was assessed by comparing the two pictures in terms of overall dark pixels present, using ImageJ software (NIH). The analysis was done blind and white noise was present during testing.

Antibodies used in this study. Rabbit anti-calretinin, Millipore (MAB1568), IHC 1:1,500 (ref. 59); rabbit anti-Cntnap4, Elior Peles (Weizmann Institute), WB 1:500 (ref. 60); mouse anti-$GABA_A$-α1, NeuroMab (75-136, clone N95/35), WB 1:1,000 (ref. 61); rabbit anti-$GABA_A$-α2, PhosphoSolutions (830-GG2), WB 1:1,000 (ref. 62); mouse anti-gephyrin Synaptic Systems (147 021, clone mAb7a), ICC 1:250 (ref. 63); mouse anti-gephyrin, Synaptic Systems (147 111, clone 3B11), WB 1:1,000 (ref. 64); rat anti-GFP, Nacalai-Tesque (04404-84, clone GF090R), IHC 1:2,000 (ref. 65); goat anti-GFP, Rockland (600-101-215), IHC 1:2,000 (ref. 65); mouse anti-N-cadherin, BD Pharmingen (561553, clone 8c11), WB 1:1,000 (ref. 66); rabbit anti-neuropeptide Y, Immunostar (22940), IHC 1:500 (ref. 67); mouse anti-parvalbumin, Sigma (P3088, clone PARV-19), IHC 1:1,000 (ref. 67); guinea pig anti-parvalbumin, David Lewis (Univ. Pittsburgh), IHC 1:1,000 (ref. 68); mouse anti-PSD-95, NeuroMab (75-348, clone K28/74), WB 1:1,000 (ref. 69); mouse anti-reelin, MBL (D223-3, clone R3b9), IHC 1:500 (ref. 70); rat anti-somatostatin, Chemicon (MAB354), IHC 1:250 (ref. 71); rabbit anti-tyrosine hydroxylase, Pel Freez (P040101), IHC 1:1,000 (ref. 72); rabbit anti-vasointestinal peptide, Immunostar (20077), IHC 1:500 (ref. 65).

31. Glessner, J. T. *et al.* Autism genome-wide copy number variation reveals ubiquitin and neuronal genes. *Nature* **459,** 569–573 (2009).

32. Elia, J. *et al.* Genome-wide copy number variation study associates metabotropic glutamate receptor gene networks with attention deficit hyperactivity disorder. *Nature Genet.* **44,** 78–84 (2012).
33. Glessner, J. T. *et al.* Strong synaptic transmission impact by copy number variations in schizophrenia. *Proc. Natl Acad. Sci. USA* **107,** 10584–10589 (2010).
34. Karayiorgou, M. *et al.* Phenotypic characterization and genealogical tracing in an Afrikaner schizophrenia database. *Am. J. Med. Genet. B. Neuropsychiatr. Genet.* **124B,** 20–28 (2004).
35. Abecasis, G. R. *et al.* Genomewide scan in families with schizophrenia from the founder population of Afrikaners reveals evidence for linkage and uniparental disomy on chromosome 1. *Am. J. Hum. Genet.* **74,** 403–417 (2004).
36. Xu, B. *et al.* Strong association of *de novo* copy number mutations with sporadic schizophrenia. *Nature Genet.* **40,** 880–885 (2008).
37. Xu, B. *et al.* Elucidating the genetic architecture of familial schizophrenia using rare copy number variant and linkage scans. *Proc. Natl Acad. Sci. USA* **106,** 16746–16751 (2009).
38. Purcell, S. *et al.* PLINK: a tool set for whole-genome association and population-based linkage analyses. *Am. J. Hum. Genet.* **81,** 559–575 (2007).
39. Li, Y., Willer, C. J., Ding, J., Scheet, P. & Abecasis, G. R. MaCH: using sequence and genotype data to estimate haplotypes and unobserved genotypes. *Genet. Epidemiol.* **34,** 816–834 (2010).
40. Li, M., Boehnke, M. & Abecasis, G. R. Joint modeling of linkage and association: identifying SNPs responsible for a linkage signal. *Am. J. Hum. Genet.* **76,** 934–949 (2005).
41. Li, M., Boehnke, M. & Abecasis, G. R. Efficient study designs for test of genetic association using sibship data and unrelated cases and controls. *Am. J. Hum. Genet.* **78,** 778–792 (2006).
42. Feinberg, K. *et al.* A glial signal consisting of gliomedin and NrCAM clusters axonal Na^+ channels during the formation of nodes of Ranvier. *Neuron* **65,** 490–502 (2010).
43. Spiegel, I. *et al.* A central role for Necl4 (SynCAM4) in Schwann cell-axon interaction and myelination. *Nature Neurosci.* **10,** 861–869 (2007).
44. Spiegel, I., Salomon, D., Erne, B., Schaeren-Wiemers, N. & Peles, E. Caspr3 and Caspr4, two novel members of the Caspr family are expressed in the nervous system and interact with PDZ domains. *Mol. Cell. Neurosci.* **20,** 283–297 (2002).
45. Jordan, B. A. *et al.* Identification and verification of novel rodent postsynaptic density proteins. *Mol. Cell. Proteomics* **3,** 857–871 (2004).
46. Phillips, G. R. *et al.* The presynaptic particle web: ultrastructure, composition, dissolution, and reconstitution. *Neuron* **32,** 63–77 (2001).
47. Restituito, S. *et al.* Synaptic autoregulation by metalloproteases and gamma-secretase. *J. Neurosci.* **31,** 12083–12093 (2011).
48. Patel, J. C. & Rice, M. E. Monitoring axonal and somatodendritic dopamine release using fast-scan cyclic voltammetry in brain slices. *Methods Mol. Biol.* **964,** 243–273 (2013).
49. Patel, J. C., Rossignol, E., Rice, M. E. & Machold, R. P. Opposing regulation of dopaminergic activity and exploratory motor behavior by forebrain and brainstem cholinergic circuits. *Nature Commun.* **3,** 1172 (2012).
50. Li, X. *et al.* Enhanced striatal dopamine transmission and motor performance with LRRK2 overexpression in mice is eliminated by familial Parkinson's disease mutation G2019S. *J. Neurosci.* **30,** 1788–1797 (2010).
51. Nicholson, C. & Patel, J. A Simplified Analysis of Dopamine Uptake by Michaelis–Menten Kinetics in *Monitoring Molecules in Neuroscience, Proceedings of the 13th International Conference on In Vivo Methods* (eds Westerink, B. *et al.*) 328–330 (Vrije Universiteit Brussel, 2010).
52. Rice, M. E., Patel, J. C. & Cragg, S. J. Dopamine release in the basal ganglia. *Neurosci.* **198,** 112–137 (2011).
53. Osten, P. *et al.* The AMPA receptor GluR2 C terminus can mediate a reversible, ATP-dependent interaction with NSF and α- and β-SNAPs. *Neuron* **21,** 99–110 (1998).
54. MacAskill, A. F. *et al.* Miro1 is a calcium sensor for glutamate receptor-dependent localization of mitochondria at synapses. *Neuron* **61,** 541–555 (2009).
55. Nikolaev, A., McLaughlin, T., O'Leary, D. D. & Tessier-Lavigne, M. APP binds DR6 to trigger axon pruning and neuron death via distinct caspases. *Nature* **457,** 981–989 (2009).
56. Foster, A. C. *et al. In vivo* pharmacological characterization of indiplon, a novel pyrazolopyrimidine sedative-hypnotic. *J. Pharmacol. Exp. Ther.* **311,** 547–559 (2004).
57. Hoeffer, C. A. *et al.* Removal of FKBP12 enhances mTOR-Raptor interactions, LTP, memory, and perseverative/repetitive behavior. *Neuron* **60,** 832–845 (2008).
58. Thomas, A. *et al.* Marble burying reflects a repetitive and perseverative behavior more than novelty-induced anxiety. *Psychopharmacol.* **204,** 361–373 (2009).
59. Miyoshi, G., Butt, S. J. B., Takebayashi, H. & Fishell, G. Physiologically distinct temporal cohorts of cortical interneurons arise from telencephalic Olig2-expressing precursors. *J. Neurosci.* **27,** 7786–7798 (2007).
60. Spiegel, I., Salomon, D., Erne, B., Schaeren-Wiemers, N. & Peles, E. Caspr3 and Caspr4, two novel members of the Caspr family are expressed in the nervous system and interact with PDZ domains. *Mol. Cell. Neurosci.* **20,** 283–297 (2002).
61. González, M. I., Cruz Del Angel, Y. & Brooks-Kayal, A. Down-regulation of gephyrin and $GABA_A$ receptor subunits during epileptogenesis in the CA1 region of hippocampus. *Epilepsia* **54,** 616–624 (2013).
62. Brandon, N. J. *et al.* A-kinase anchoring protein 79/150 facilitates the phosphorylation of $GABA_A$ receptors by cAMP-dependent protein kinase via selective interaction with receptor β subunits. *Mol. Cell. Neurosci.* **22,** 87–97 (2003).
63. Panzanelli, P. *et al.* Distinct mechanisms regulate $GABA_A$ receptor and gephyrin clustering at perisomatic and axo-axonic synapses on CA1 pyramidal cells. *J. Physiol. (Lond.)* **589,** 4959–4980 (2011).
64. Hoon, M. *et al.* Neuroligin 2 controls the maturation of GABAergic synapse and information processing in the retina. *J. Neurosci.* **29,** 8039–8050 (2009).
65. Miyoshi, G. *et al.* Genetic fate mapping reveals that the caudual ganglionic eminence produces a large and diverse population of superficial cortical interneurons. *J. Neurosci* **30,** 1582–1594 (2010).
66. Restituito, S. *et al.* Synaptic autoregulation by metalloproteases and γ-secretase. *J. Neurosci.* **31,** 12083–12093 (2011).
67. Batista-Brito, R. *et al.* The cell-intrinsic requirement of Sox6 for cortical interneuron development. *Neuron* **63,** 466–481 (2009).
68. Condé, F., Lund, J. S., Jacobowitz, D. M., Baimbridge, K. G. & Lewis, D. A. Local circuit neurons immunoreactive for calretinin, calbindin D-28k or parvalbumin in monkey prefrontal cortex: distribution and morphology. *J. Comp. Neurol.* **341,** 95–116 (1994).
69. Belzil, C. *et al.* A Ca^{2+}-dependent mechanism of neuronal survival mediated by the microtubule-associated protein p600. *J. Biol. Chem.* **288,** 24452–24464 (2013).
70. Miyoshi, G. & Fishell, G. Dynamic *FoxG1* expression coordinates the integration of multipolar pyramidal neuron precursors into the cortical plate. *Neuron* **74,** 1045–1058 (2012).
71. Close, J. *et al.* Satb1 is an activity-modulated transcription factor required for the terminal differentiation and connectivity of medial ganglionic eminence-derived cortical interneurons. *J. Neurosci.* **32,** 17690–17705 (2012).
72. Haycock, J. W. Stimulation-dependent phosphorylation of tyrosine hydroxylase in rat corpus striatum. *Brain Res. Bull.* **19,** 619–622 (1987).

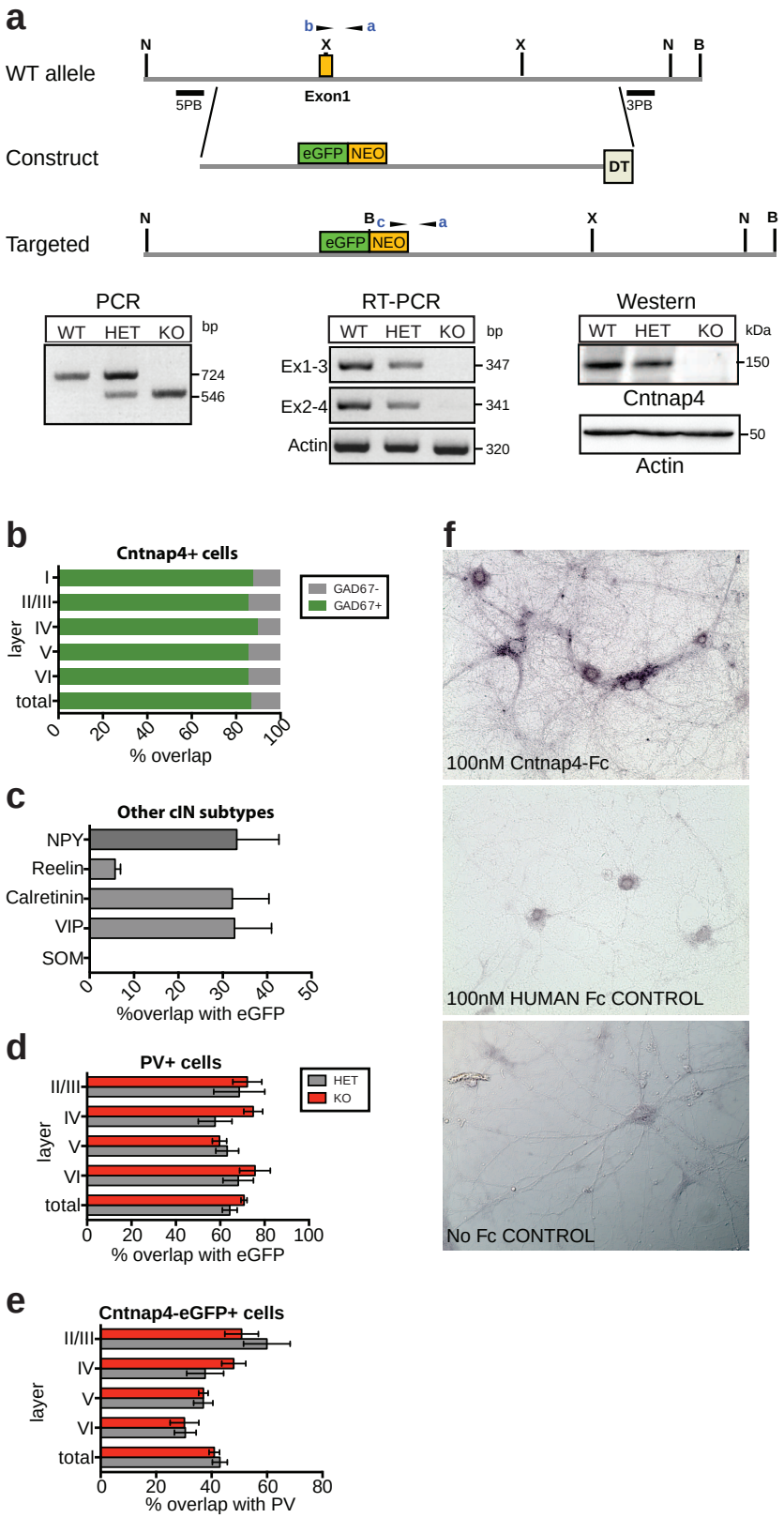

Extended Data Figure 1 | Generation of *Cntnap4* knockout (KO) mice and localization of the gene and the protein. **a**, Schematic representation of targeting strategy to generate mutant eGFP-knock-in knockout *Cntnap4* allele. Primers used for genotyping (a–c) are indicated. X, XhoI, H, NheI, B, BahmHI sites. PCR, RT–PCR and western blot show correct gene targeting, disrupted transcription and translation of Cntnap4, respectively. **b**, Distribution of Cntnap4-positive cells that are also GAD67 positive by layer in a double fluorescent *in situ* hybridization analysis ($n = 2$ brains). **c**, Percentage of overlap between interneuron markers (NPY, reelin, calretinin and VIP) and *Cntnap4*-eGFP. **d**, **e**, Percentage of overlap between PV and *Cntnap4*-eGFP across all layers (**b**–**d**, bars represent the mean; error bars, s.e.m.; $n = 4$ brains). **f**, Cntnap4–Fc *in vitro* labelling and controls. Colorimetric detection of a human Fc-tagged Cntnap4 extracellular domain on live dissociated hippocampal neuronal cultures (top image). No specific binding or signal upon application of human-Fc negative control (middle panel) or with no human Fc present (bottom panel) ($n = 4$ cultures, 2 replicates each).

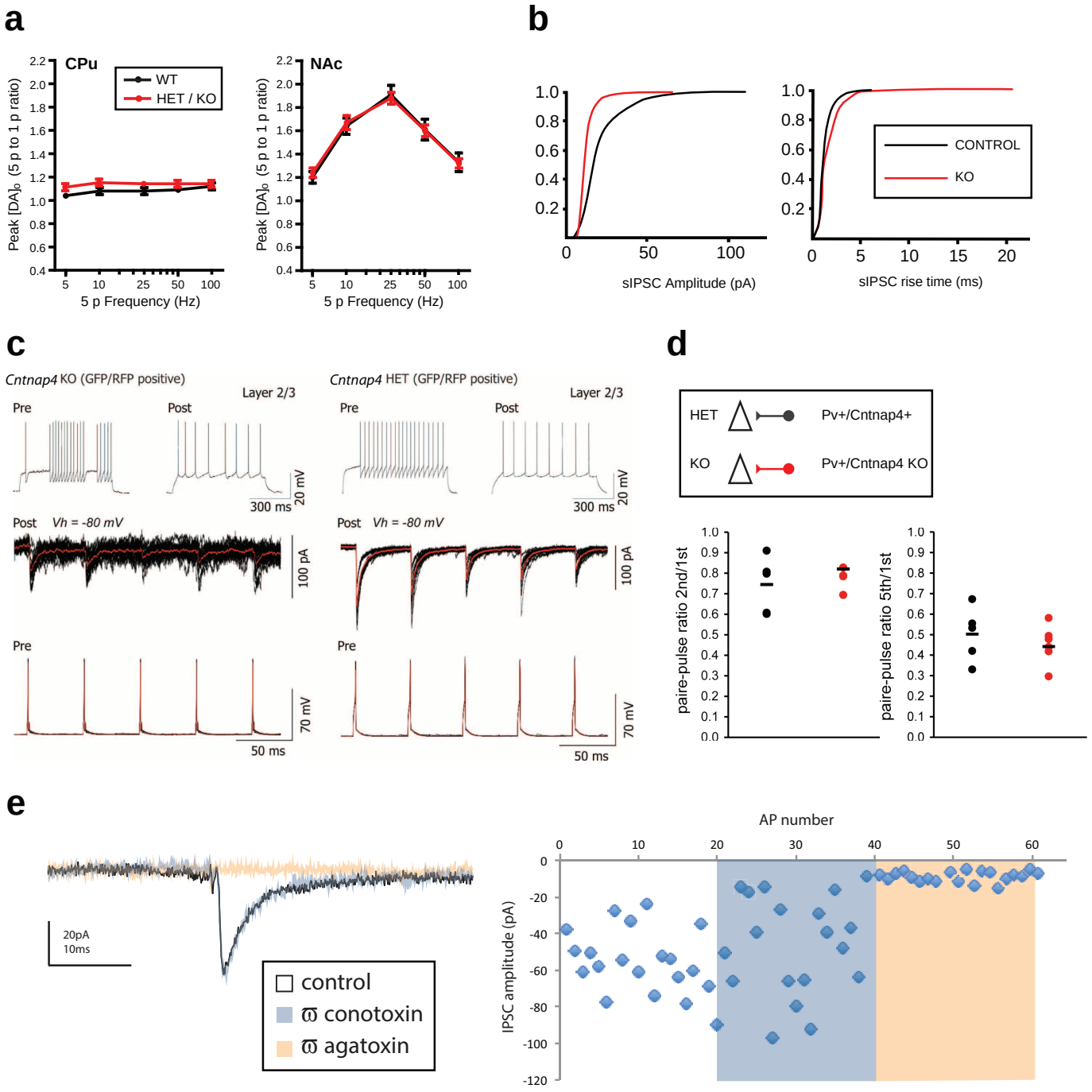

Extended Data Figure 2 | Presynaptic measures for dopaminergic and GABAergic transmission. **a**, Voltammetric monitoring of extracellular [DA]o in the CPu and NAc of striatal slices. Frequency dependence (5 p-to-1 p ratio) of evoked [DA]o in WT and mutant *Cntnap4* mice (HET/KO) was not different across frequencies (5, 10, 15, 50, 100 Hz; $n = 4$ per genotype; two-way ANOVA, post-hoc Bonferroni test). **b**, Cumulative distributions of spontaneous inhibitory postsynaptic current (sIPSC) amplitude and rise time recorded from P17–P21 control ($n = 8$ cells) and *Cntnap4* KO ($n = 7$ cells) layer 2/3 pyramidal cells *in vitro*. Kolmogorov–Smirnov test used for statistical analysis. **c**, Series of evoked synaptic IPSCs recorded in RS pyramidal cells at 20 Hz (below) in HET (right) versus KO *Cntnap4* mice (left). Average trace in red with black individual traces (10 sweeps). **d**, Plots showing the paired pulse ratios calculated for the first and second and the first and fifth responses in the synaptic train (HET: $n = 4$ brains, $n = 8$ cells; KO: $n = 4$ brains, $n = 11$ cells; unpaired *t*-test used to compare groups statistically) **e**, Loss of *Cntnap4* does not alter pre-synaptic calcium channel type dependence for synaptic release. IPSCs completely blocked by the P/Q-type blocker ω−agatoxin (100 μM), not altered by the N-type blocker ω−conotoxin (200 μM) ($n = 3$ brains, $n = 3$ cells).

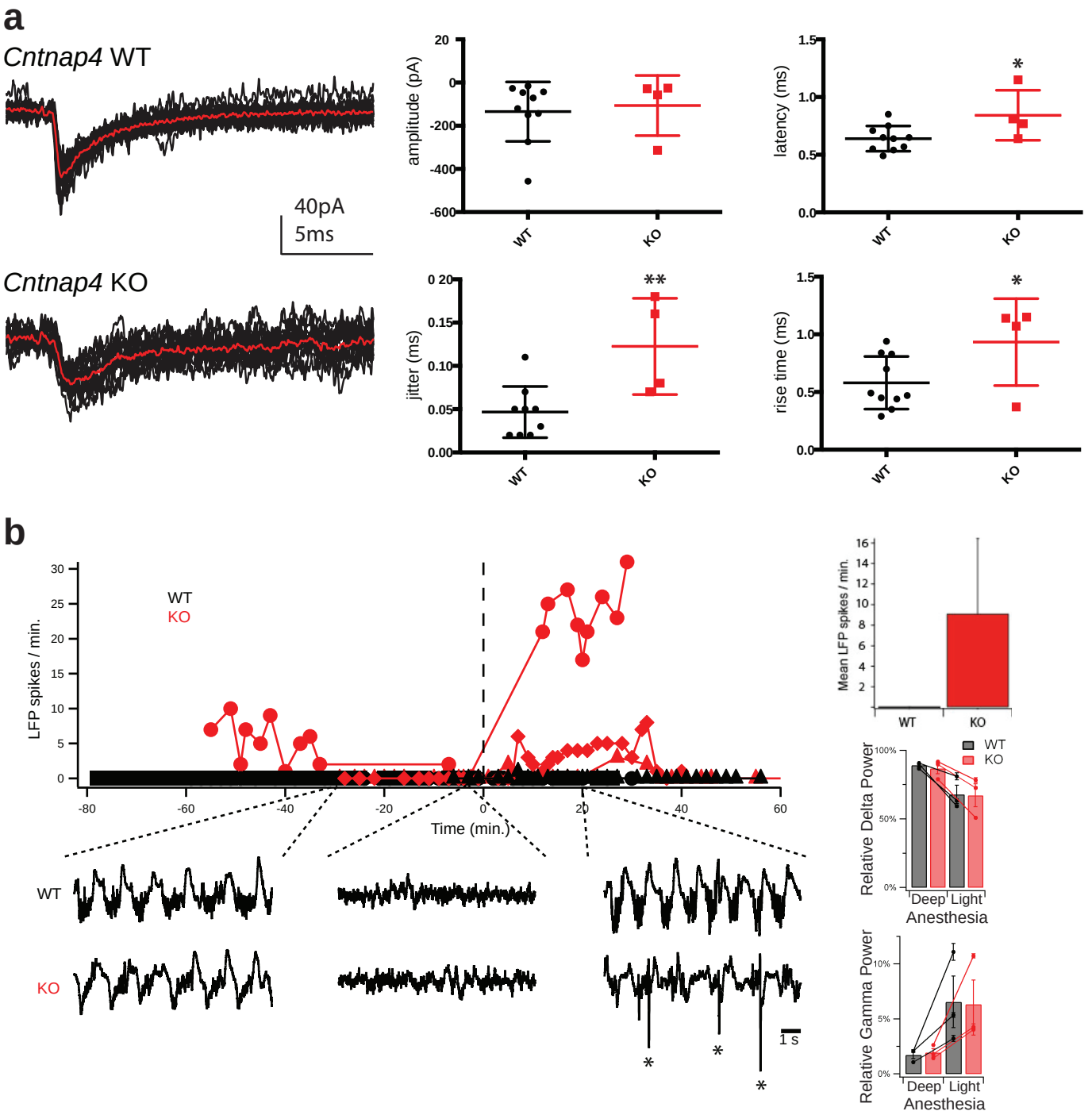

Extended Data Figure 3 | FS to pyramidal cell synaptic transmission deficits persist into adulthood in *Cntnap4* KO mice by *in vitro* slice physiology and mild epileptiform-like discharges observed in vivo under anaesthesia. **a**, Examples of FS evoked IPSCs from adult *Cntnap4* WT and KO mice (P60–P90), showing that the latter remain immature (unpaired *t*-test, $*P < 0.05$, $**P < 0.01$, $***P < 0.005$. WT: $n = 2$ brains, $n = 10$ pairs; KO: $n = 1$ brain; $n = 4$ pairs). **b**, Graph depicting the number of LFP spikes per minute over the time course of the *in vivo* recordings of 3 wild type (WT: black circle, triangle and diamond) and 3 knock out (KO: red circle, triangle and diamond) adult mice. Time 0 is the time a large injection of ketamine/xylazine was given, bringing the animal back into deep anaesthesia. Example traces from LFP signals of a WT and a KO mouse taken sequentially under deep, light and deep anaesthesia are shown underneath (asterisks mark spikes). Bar graph of the average number of LFP spikes per min shows absence of spikes in WT animals. Calculated relative power (relative power = band power/total power) for delta (0.5–4 Hz) and gamma (20–80 Hz) frequency bands are shown underneath for light and deep anaesthesia. No statistically significant effect of genotype on the relative power in either frequency band was detected (three-way ANOVA performed with animal ID as factor within genotype on gamma and delta power).

a

		Vrm (mV)	Rin (MOhm)	Cm (pF)	tau (ms)	I to AP (pA)	AP thresh. (mV)	AP ampl. (mV)	AP width (ms)	AHP amplit. (mV)	delay to 1st AP (ms)	sag (mV)	max firing (Hz)
WT (n=7)	avg	-65.00	114.92	0.05	6.07	226.17	-39.34	73.75	0.34*	20.36	136.20	1.93	277.00
	sem	1.89	12.19	0.01	0.74	35.93	2.36	1.32	0.02	3.17	69.00	0.50	15.07
HET (n=10)	avg	-65.20	166.38	0.05	8.19	136.90	-33.38	69.18	0.42	23.10	153.74	3.16	260.75
	sem	1.14	13.62	0.00	0.52	15.74	2.57	5.34	0.02	1.91	43.18	0.80	8.53
KO (n=9)	avg	-67.22	215.61	0.05	9.35	128.44	-31.85	63.55	0.47	27.48	242.13	3.37	248.57
	sem	1.53	56.93	0.01	2.55	22.75	1.09	4.42	0.04	1.05	60.28	0.50	15.96

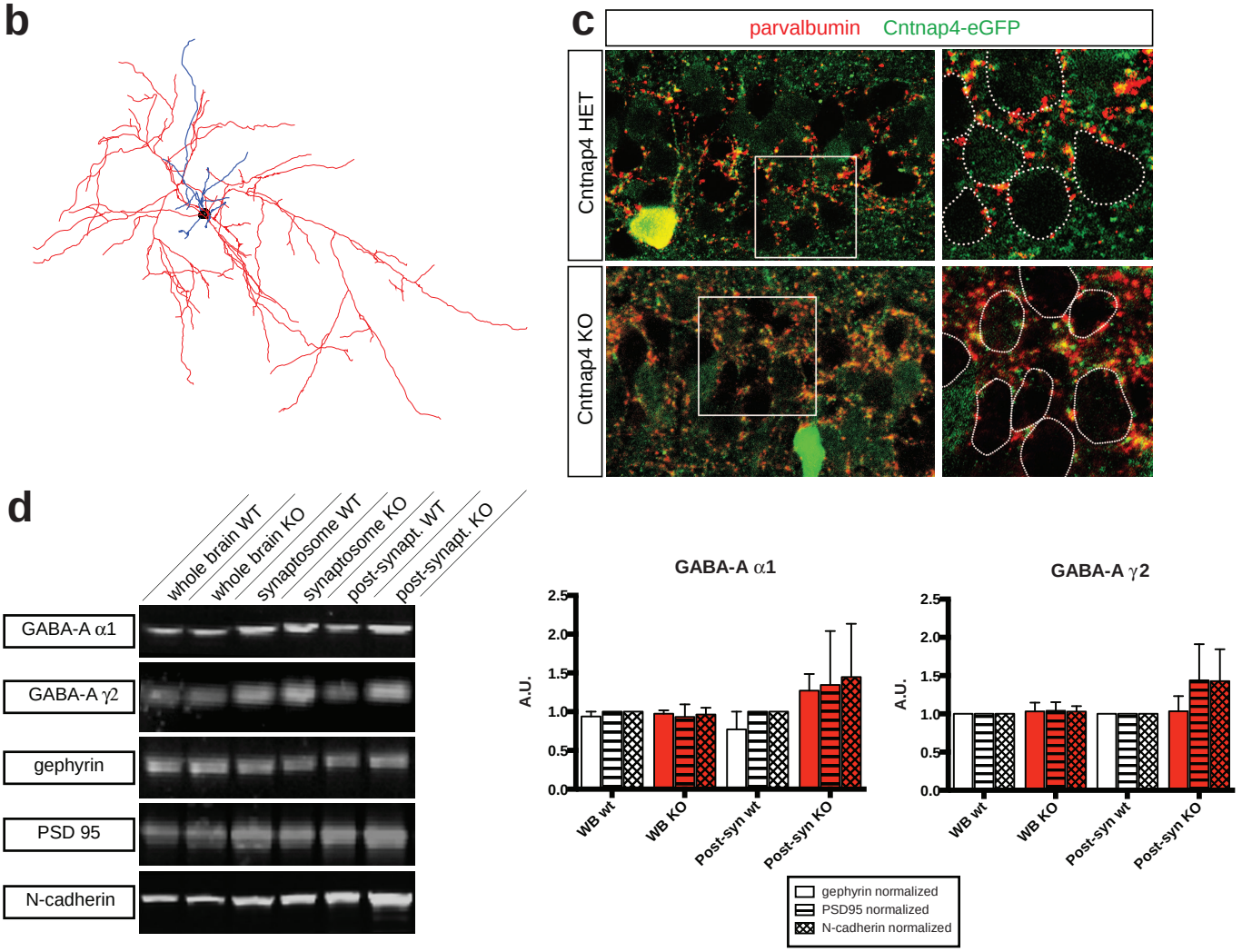

Extended Data Figure 4 | Intrinsic electrophysiological properties, morphology and localization of postsynaptic $GABA_A$ receptors in *Cntnap4* WT and KO mice. **a**, No differences were detected in the passive or active membrane properties of fast spiking (FS) basket cells in the *Cntnap4* HET versus *Cntnap4* KO mice. (WT: $n = 2$ brains, $n = 7$ cells; HET: $n = 6$ brains, $n = 10$ cells; KO: $n = 4$ brains, $n = 9$ cells; ANOVA with post hoc Tukey's test used to compare groups statistically). **b**, Reconstruction of a layer 5 *Cntnap4* KO FS cell. Soma in black, dendrites in blue and axon in red. **c**, Images of hippocampal CA1 pyramidal cell layer from *Cntnap4* HET and KO mice, showing normal perisomatic labelling of parvalbumin-positive terminals. The images were also stained for eGFP (*Cntnap4*) staining. The closed dotted lines show the position of cell somata. **d**, Representative blots of $GABA_A$-α1, $GABA_A$-γ2, gephyrin, PSD 95 and N-cadherin of various brain fractions. Bar graphs showing $GABA_A$-α1 levels quantified and normalized to gephyrin, PSD-95 and N-cadherin loading controls. Also shown are $GABA_A$-γ2 levels quantified and normalized to gephyrin, PSD-95 and N-cadherin loading controls ($n = 3$ biological replicates).

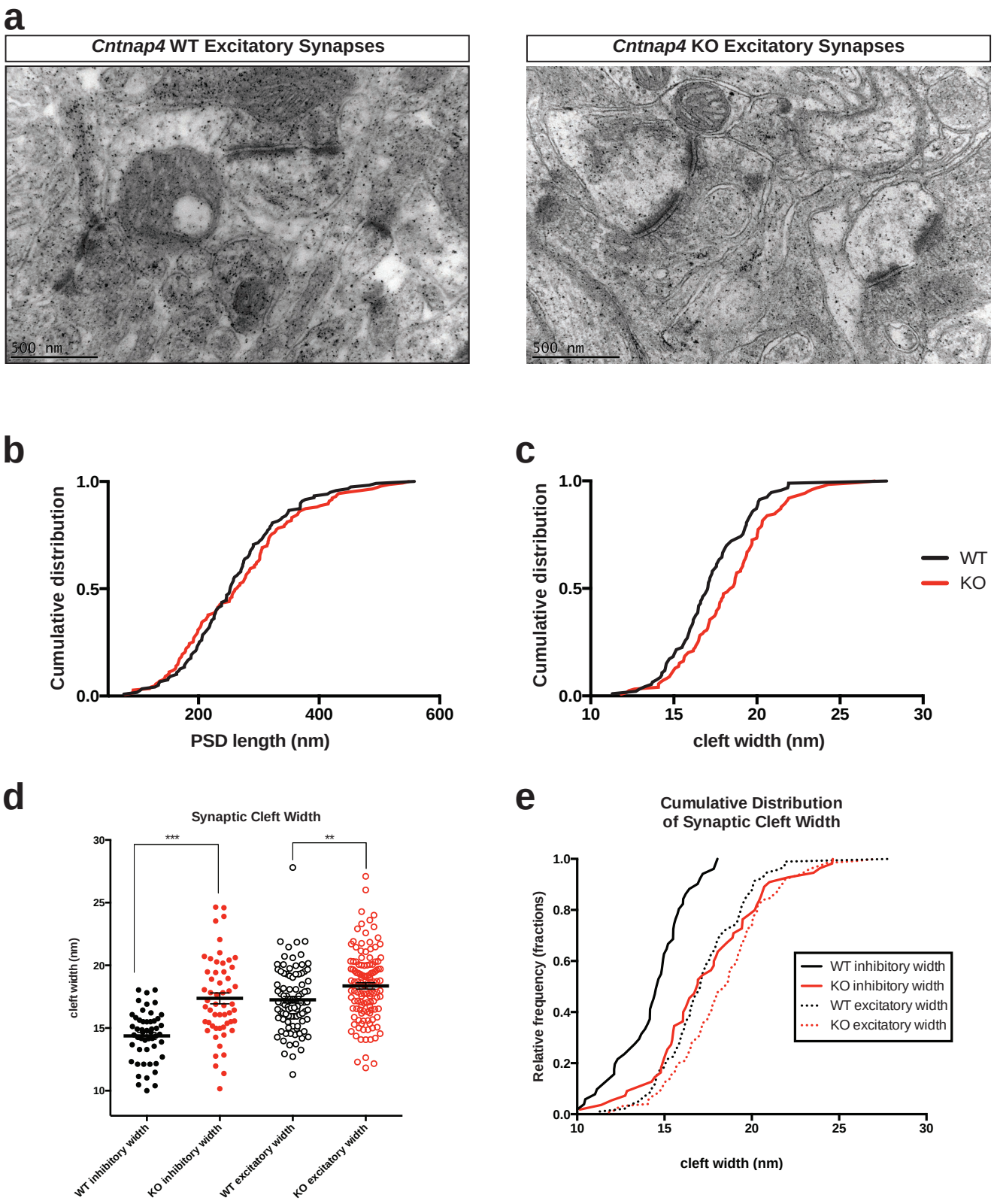

Extended Data Figure 5 | Ultrastructural analysis of excitatory synapses between WT and KO animals. **a**, Representative electron micrographs of *Cntnap4* WT and KO excitatory synapses at ×57 000 magnification. **b**, **c**, Postsynaptic density length (**b**) and cleft width (**c**) of excitatory synapses in the SSBF1 of *Cntnap4* WT and KO mice. A statistically significant difference in cleft was observed in *Cntnap4* KO compared to the WT mice ($P = 0.0089$). PSD length of excitatory synapses however, was unchanged between KO and WT. **d**, Dot plot comparison of inhibitory versus excitatory synapses across WT and KO. The relative effect of *Cntnap4* loss is much more pronounced in inhibitory synapses. **e**, This effect is also readily apparent when the data sets are represented by culmulative distribution. (**d, e**, $^{**}P < 0.01$; $^{***}P < 0.001$, Kolmogorov–Smirnov test for width). (**b**–**e**: $n = 2$ brains for each genotype; width: WT $n = 93$ synapses; KO $n = 124$ synapses; length: WT $n = 119$ synapses; KO $n = 143$ synapses).

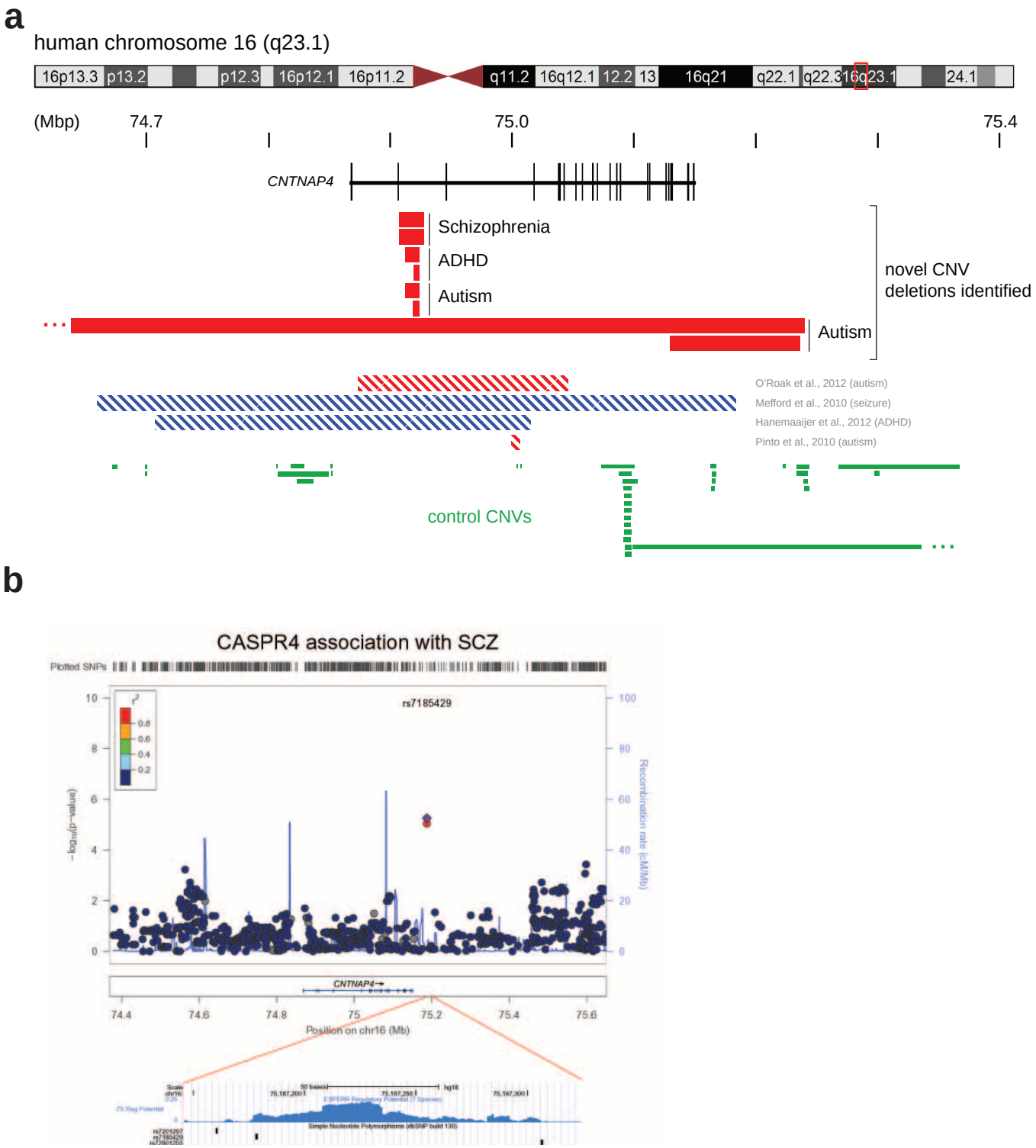

Extended Data Figure 6 | Human genetics data implicating *CNTNAP4* in neuropsychiatric disorders. **a**, Novel and published CNVs present in the *CNTNAP4* locus on human chromosome 16. We identified eight new cases of human individuals with neuropsychiatric disorders (2 with schizophrenia, 4 with ASD and 2 with ADHD). Six of these individuals had CNVs in the second intron of the gene (top), whereas two had larger exonic deletions in *CNTNAP4* (bottom). Previously reported cases of deletions (red striped) or duplications (blue striped) within the gene are presented underneath. Green bars depict CNVs in the *CNTNAP4* gene and proximal regions on either side of it found in control non-afflicted individuals. **b**, Two *CASPR4* (*CNTNAP4*) single nucleotide polymorphisms (SNPs) associating with schizophrenia (SCZ) were found to have gene-wide significant association (rs7185429 and rs7201297). The region containing the two SNPs is shown below in light blue (Schizophrenia-GWAS-SNP). The plot depicts the association *P* values of SNPs within *CNTNAP4* in SCZ families (top). Both SNPs reside in a region predicted to be regulatory by the ESPERR Regulatory Potential program (http://www.genome.ucsc.edu). ESPERR regulatory potential based on 7 species (bottom).

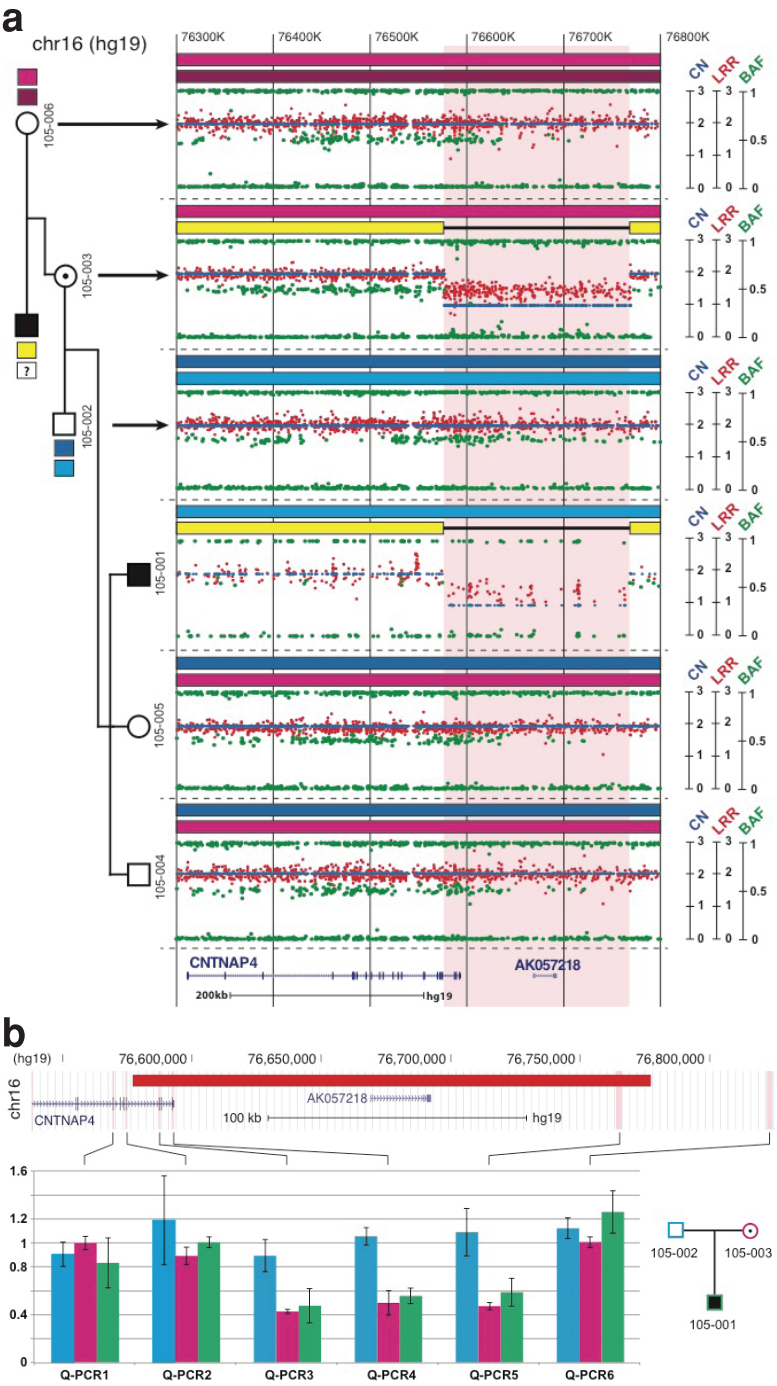

c

Name	chr	Start	Stop	Size (bp)	Forward (5'-3')	Tm(°C)	Reverse (5'-3')	Tm(°C)
Q-PCR1_16_76569450_76569614	16	76569450	76569614	165	gccaccagacagagaggc	59.5	tctgcatttccctccattg	59.6
Q-PCR2_16_76574523_76574679	16	76574523	76574679	157	tgtcctctgttgcttcctgtc	60.4	ctgcccaataccagagatttg	59.6
Q-PCR3_16_76587261_76587391	16	76587261	76587391	131	acgtggcccctctgaag	59.8	cgagtgtgtcctttcccttg	60.7
Q-PCR4_16_76592386_76592530	16	76592386	76592530	145	ggtctgatagctgttgtgatttttatc	60.6	gctcacttttcagaacagcctc	60.6
Q-PCR5_16_76756056_76756205	16	76756056	76756205	150	gaagtgaagtgcctgaaaatttc	59.3	gattctaacaaacagcttgctttg	59.5
Q-PCR6_16_76825824_76825993	16	76825824	76825993	170	gtggctggactcaacaattg	59.1	ctcaacacgatggggaatg	59.9

Extended Data Figure 7 | Identification of a heterozygous deletion of *CNTNAP4*. **a**, All family members, except the grandfather with Asperger syndrome, were genotyped using the Illumina Human Omni 1 SNP array. The patient with Asperger syndrome (105-001) and his mother were carrying a 191 kb deletion on chromosome 16q13.3 including the 3 last exons of *CNTNAP4* and the AK057218 gene. Based on informative SNPs located within the deletion, we ascertained that the deletion was on the grandfather's chromosome. This grandfather was diagnosed with Asperger syndrome, but DNA was not available to ascertain if he was carrying the deletion or if the deletion appeared *de novo* in his daughter (105-003). Each dot shows Log R Ratio (LRR; in red), the B allele frequency (BAF; in green) and the copy number (CN; in blue). **b**, The *CNTNAP4* deletion was validated by quantitative PCR. Results obtained on the genomic DNA from the proband (105-001), his parents, and two controls confirmed that the deletion was inherited from the mother and removed the 3 last exons of *CNTNAP4*. Bars represent mean of RQ ± s.e.m. **c**, Primers used for the *CNTNAP4* CNV validation by quantitative PCR.

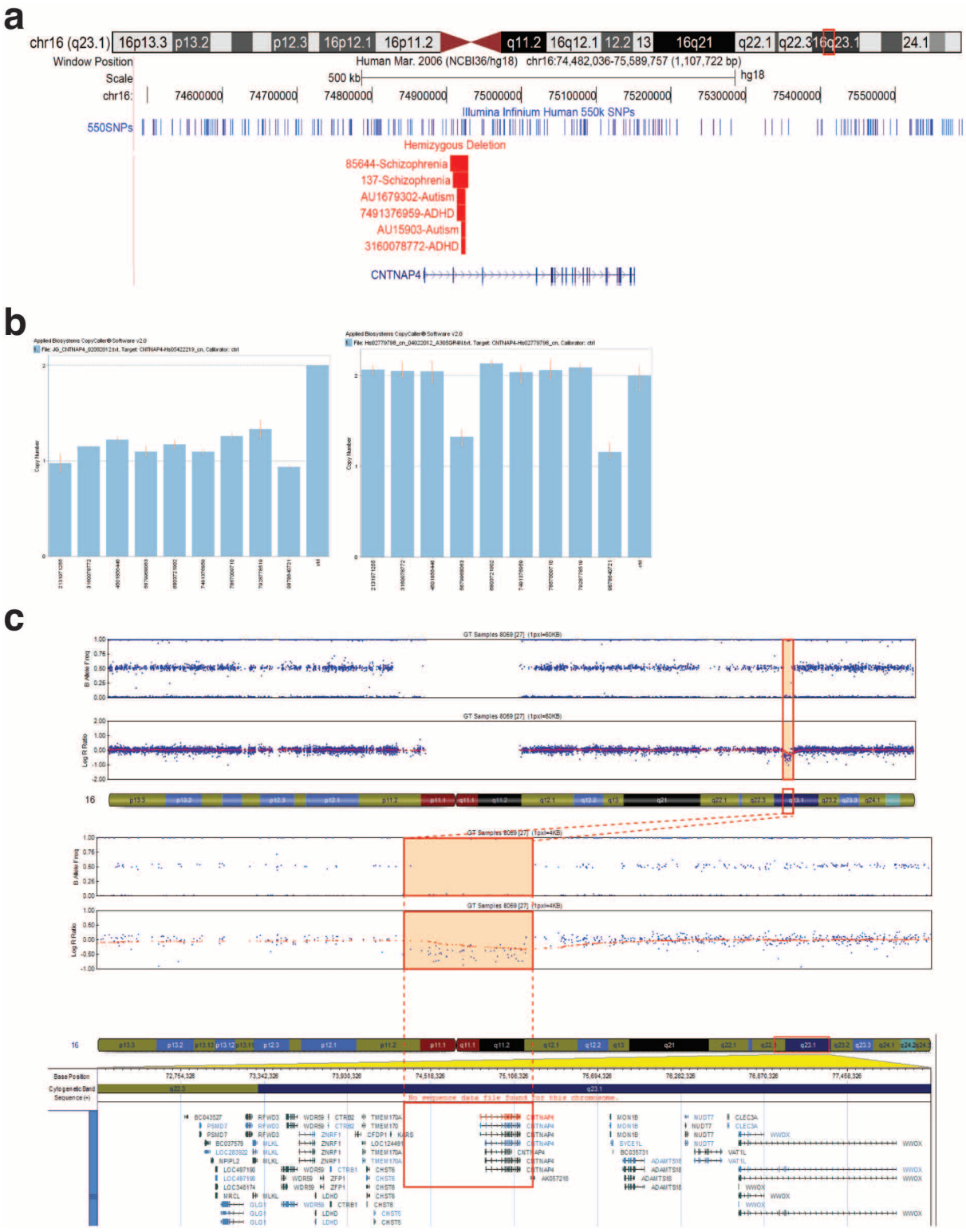

Extended Data Figure 8 | Identification and validation of *CNTNAP4* intronic and exonic deletions in individuals with neuropsychiatric disorders. **a**, *CNTNAP4* chromosome 16 (chr16): 74,482,036–75,589,757 with Illumina Infinium Human 550K SNPs coverage displayed as dark blue lines across the top. CNVs are shown in red for hemizygous deletions. All intron II deletions in *CNTNAP4* in the six cases are listed first, followed by two larger duplications and two deletions affecting *CNTNAP4* previously reported in the literature. **b**, All CNV calls in cases shown in **a** were positively validated by TaqMan copy number assay. **c**, An heterozygous *CNTNAP4* deletion was identified with the cytoSNP array from Illumina in family II. An individual diagnosed with autism and mild intellectual disability possesses a heterozygous deletion, maternally inherited, which spans 916.2 kb on chromosome 16q23.1 (hg19, 75,766,089–76,682,263), and includes all exons of *CNTNAP4* (delineated by the orange square). The upper plot shows B allele frequency (in blue) and the lower plot shows Log R Ratio (in red).

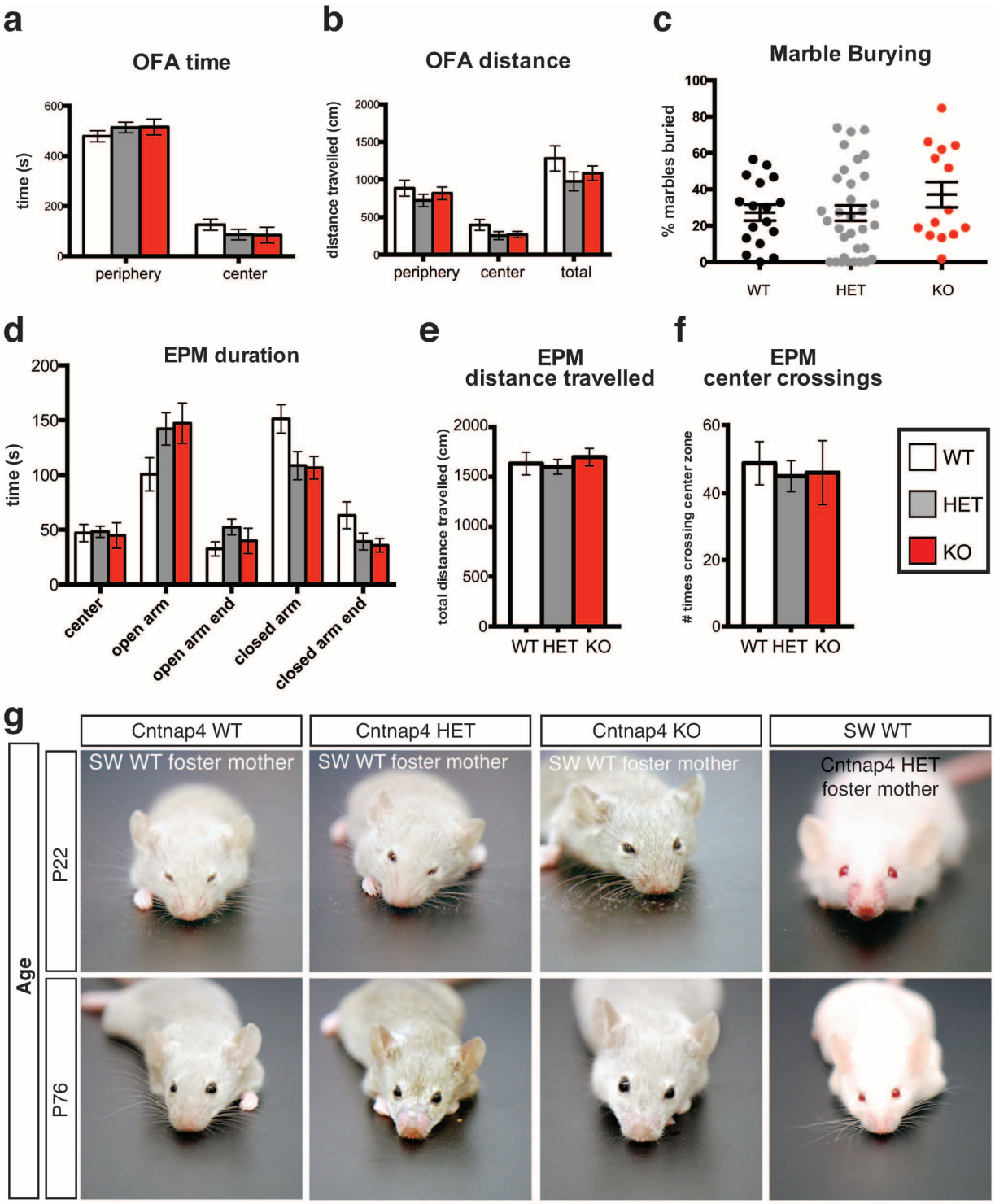

Extended Data Figure 9 | Behavioural tests in *Cntnap4* mice. **a**, **b**, No major changes in anxiety levels were observed in the mutant mice as indicated by time and distance spent in periphery versus centre in open field arena (OFA) (WT, $n = 14$; HET, $n = 13$; KO, $n = 10$). **c**, No major changes observed in extent of marble burying in the mutant versus control mice (WT, $n = 17$; HET, $n = 33$; KO, $n = 14$). **d**–**f**, No difference was found in the time spent in the open or closed arms, total distance travelled or centre crossings in the elevated plus maze (EPM) between mutants and control animals (WT, $n = 14$; HET, $n = 12$; KO, $n = 11$). **g**, Grooming tracks with the *Cntnap4* mutant allele. A series of representative images of *Cntnap4* mutant mice (Het and KO) cross-fostered by Swiss Webster wild type (SW WT) dam or SW WT mice cross-fostered onto *Cntnap4* mutant dam. Grooming status documented at two different ages: just after weaning (P22) and at P76. At P22, presence or absence of allo-grooming by the mother is apparent, whereas at P76 the presence or lack of whiskers depends on the mouse's genotype. See Methods for more detail.

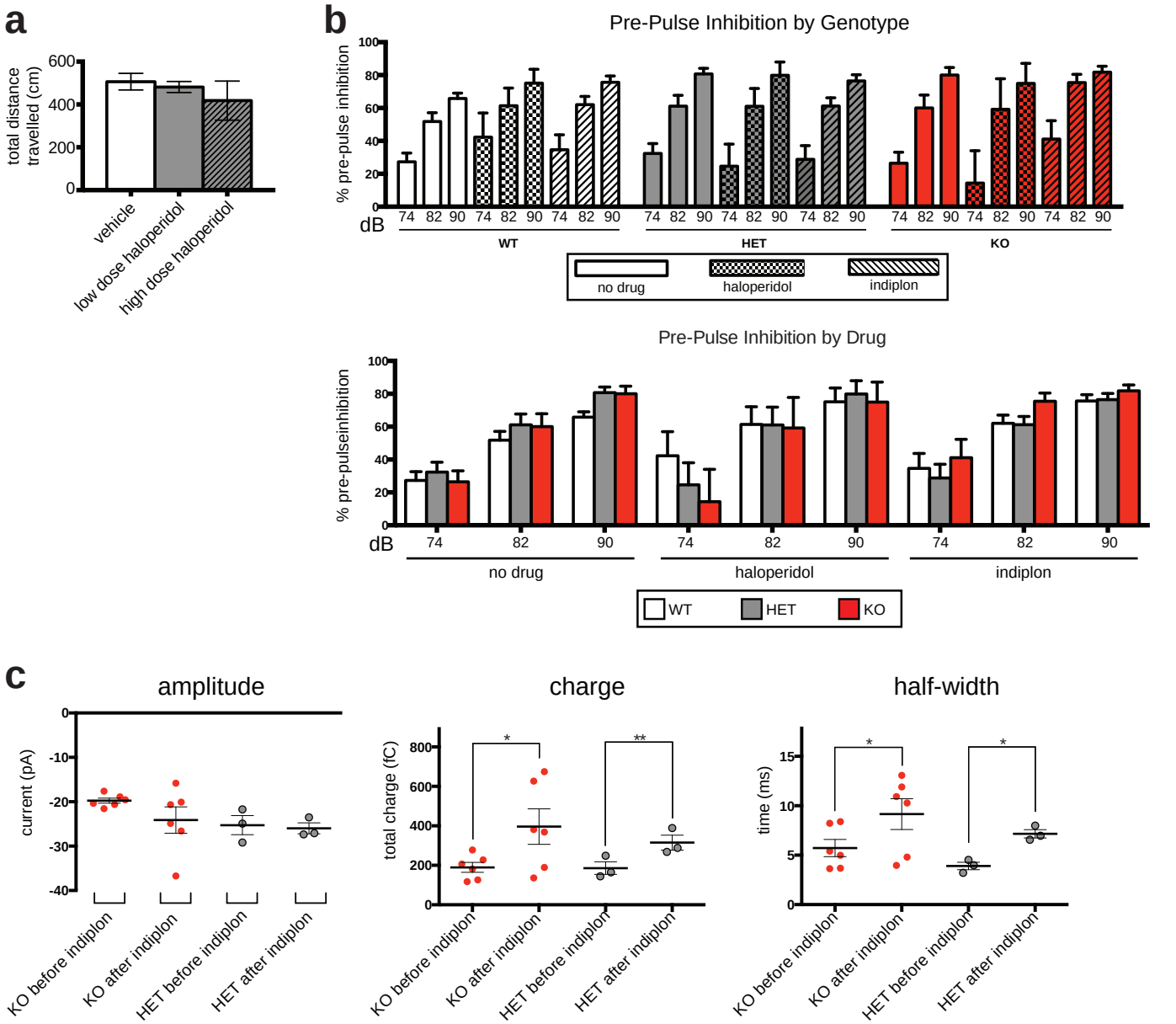

Extended Data Figure 10 | Drug effects on spontaneous IPSCs, as well as PPI and locomotion. **a**, Haloperidol administration does not lead to a significant reduction in locomotion in *Cntnap4* HET mice as measured by the total distance travelled in an open field arena (OFA) (vehicle $n = 6$ mice; low haloperidol $n = 6$ mice; high haloperidol $n = 3$ mice; ANOVA used for statistical analysis). **b**, Percentage of pre-pulse inhibition (PPI) for each genotype in control and under haloperidol and indiplon administration for a series of pre-pulses (74,82,90 dB). Below, same data re-organized by drug regimen in each genotype group. **c**, Effect of indiplon on amplitude, charge and half-width of proximal and perisomatic spontaneous IPSCs recorded from layer 2/3 P23–25 pyramidal cells of KO ($n = 3$ brains, $n = 6$ cells) and HET ($n = 1$ brain, $n = 3$) mice *in vitro*, unpaired *t*-test (*$P < 0.05$; **$P < 0.01$; ***$P < 0.001$).